Electrical Imaging of the Heart: Electrophysical Underpinnings and Signal Processing Opportunities

Dana H. Brooks[#], and Robert S. MacLeod[†]

[#]Communications and Digital Signal Processing (CDSP) Center, Electrical and Computer Engineering Department, Northeastern University, Boston, MA

[†]Cardiovascular Research and Training Institute (CVRTI),University of Utah, Salt Lake City, UT

This material is based upon work supported by the National Science Foundation under Grant No. BCS-9309359, a Biomedical Engineering Grant from the Whitaker Foundation, and support from the Nora Eccles Harrison Treadwell Foundation

May 4, 1998

Abstract

This paper describes a non-traditional medical imaging modality, cardiac electrical imaging, which is a generalization of the standard electrocardiogram (ECG). Rather than recording from a few relatively isolated leads as in the ECG, a more comprehensive and detailed image sequence of the time-varying spatial distribution of electrical potentials which originate in the heart muscle is obtained using a much larger number of electrodes. These images can be recorded non-invasively on the body surface, or, using invasive procedures, on, or even in, the heart muscle. The modality provides increased information about cardiac electrical and mechanical function, but extracting that information effectively from the images remains a challenge after 30 years of development. We describe some electrophysiological background necessary to understand the characteristics and advantages of such recordings, we describe the technical requirements of the method, we review some of the processing approaches which have been applied to aid in their interpretation, and we outline the inverse problem which relates these images to a model for the underlying cardiac sources.

1 Introduction

The electrocardiogram (ECG), a standard tool of modern clinical medicine, is a recording of the difference in electrical potential between a few electrodes placed on a person's chest and/or limbs and a reference lead or leads. Physicians have learned over the years to identify a large number of cardiac abnormalities from the ECG, but its interpretation remains more a process of heuristic pattern recognition than an analysis based on a solid biophysical model. One limitation which keeps the standard ECG from providing a more comprehensive and transparent description of the electrical state of the heart is that it is a very sparse sampling of a complicated, spatially varied distribution of potential on the body surface. The most informative regions of this distribution, such as areas of local maxima, or minima, or high gradients, might be captured by the standard electrode configuration on one person and missed on another. In addition, the information about cardiac sources contained in the ECG suffers from attenuation and smoothing due to the volume conductor which separates the heart from the body surface. Indeed, it is a tribute to the skill of human interpreters that the ECG is a common and relatively effective diagnostic tool despite these limitations—in addition it has the advantages of being cheap and painless. However there is uncertainty and error in ECG-based diagnoses—for example, the rate of false diagnosis in myocardial infarctions ("heart attacks") is as high as 30% and results in unnecessary health care costs in the U.S. estimated at $4 billion per year [1].

As we will describe below, there is a complicated interaction between the mechanical function of the heart, its internal electrical behavior, and externally recorded potentials. Failure to take these relationships into account can lead to simplistic models of how cardiac electrical activity is reflected in external potential measurements. This may in turn lead to misinterpretation, oversimplification, and failure to make full use of the available information. Important features of cardiac electrophysiology to consider include the origin and propagation of cardiac excitation, the spatially and temporally distributed nature of the resulting intracardiac wavefronts, the electrical anisotropy of cardiac tissue, the spatio-temporal relationship between intracardiac source activity and extracardiac potentials, the heterogeneous conductivity of the torso volume between the heart and the body surface, and the spatial relationship between a particular measurement location and the distributed sources.

This paper describes a body of research concerned with the application of multi-electrode arrays to partially overcome the undersampling problem together with the use of intrusive measurements and/or sophisticated processing to deal with the attenuation and smoothing. With such an array we can record an "image sequence" of electrical potentials; the goal of this recording is the acquisition, extraction, and presentation of information about the electrical activity of the heart. These potentials may be measured within, on, or very near the heart through invasive procedures, or non-invasively directly on the skin. Unlike the other medical imaging modalities described in this issue, which generally display or reconstruct either anatomical features (MRI, ultrasound, CT) or metabolic activity (PET), the idea here is to image or reconstruct electrical activity itself; anatomical features, represented in a geometric model, are not the end product but rather an essential prerequisite of the method, necessary to provide an underlying structure upon which to display, understand, and analyze electrophysiological quantities. The ultimate objectives of this modality are twofold:

1. **increased basic knowledge**, helping scientists to better understand the normal and abnormal electrical activity of the heart, and

2. **clinical applications**, developing improved or new tools that apply this knowledge to the diagnosis and monitoring of patients.

This modality, known as "cardiac electrical imaging" or "cardiac mapping", involves acquisition and management of both anatomical and electrical data. Specific technical requirements include registration and segmentation of the anatomical data and data storage, compression, and visualization of both anatomical and electrical data. Image and signal processing can also play a role in image representation, compression, and feature extraction, as well as in aiding integration of imaging results with the underlying biophysics and physiology to facilitate accurate interpretation of the images. Specific relevant problems include image restoration (inverse solutions) and the development of physiologically meaningful measures of similarity between image sequences.

The complexity of electrocardiographic imaging data, and of the underlying biophysical models, require more sophisticated analysis methods than the empirical techniques generally used on the immense number of ECGs recorded in clinical practice (parameter extraction, pattern recognition and heuristic evaluation or scoring systems [2, 3, 4]). Given the significant additional demands of electrocardiographic imaging, the required effort and cost must be justified from either a research or a clinical perspective. The initial rationale for acquiring potentials from the entire torso surface (body surface potential mapping, or BSPM) was to evaluate the nature of cardiac source models, and in particular the degree to which a single current dipole embedded in the chest could represent net cardiac bioelectric fields on the body surface [5]. Data from BSPM revealed the inadequacies of the single dipole model and subsequent studies have demonstrated the utility of BSPM in diagnosing a range of clinical conditions including coronary artery disease [6, 7] myocardial infarctions [8, 9], cardiac arrhythmias [10, 11] and left ventricular hypertrophy [12]. Persistent barriers to widespread use of cardiac electrical imaging in clinical cardiology are mainly the practical problem of applying 32–200 electrodes to a patient and the weaknesses of the analysis methods developed to date. That electrocardiographic imaging obtains more information than ECG's is of little doubt, as shown by the widespread research use of the technique. However significant challenges remain in information processing, extraction, and presentation, to facilitate better scientific interpretation and more widespread clinical application.

In the rest of the paper we first describe some relevant background electrophysiology and then give an overview of the technical challenges which arise in displaying, representing, and analyzing these images. The bibliography section is necessarily not exhaustive, so the references should each be regarded as typical of a class of methods rather than representing an exhaustive listing. In addition space considerations have forced us to omit a number of valuable approaches; we apologize in advance to those researchers whose work we may have neglected. Among the important topics which we have not treated are defibrillation (see [13]), optical mapping [14], and segmentation/detection/classification of ECG waveforms.

2 Background Electrophysiology

From an engineering viewpoint, we can consider the heart as a closed, electrically conducting shell of non-negligible thickness that contains electrical sources. This shell is composed of muscle cells which have three properties of importance here: they are capable of generating a dramatic change in the electrical potential difference across the cell membrane, known as an *action potential* (AP); they can propagate the impetus to generate an action potential to neighboring cells, thus producing a *moving wavefront* of spatially varying electric potential; and they *contract* mechanically if their intracellular calcium ion concentration increases. Since, in fact, just such an increase in calcium concentration occurs as part of each action potential, the electrical and mechanical aspects of the heart's functionality are intimately linked: electrical events lead directly to mechanical action but mechanical events can also (usually subtly) alter subsequent electrical behavior. Abnormalities or

changes in either can cause abnormalities or changes in the other—thus, by measuring potentials resulting from cardiac electrical sources, we can obtain important information about the health of the heart muscle. In addition, certain aspects of cardiac function and disfunction are characterized uniquely by electrical behavior. For instance, changes in the sequence of a part of the electrical cycle known as the recovery (repolarization) phase are not necessarily immediately reflected in mechanical alterations, yet there is evidence that they increase the risk for the most serious heart rhythm disturbance, ventricular fibrillation [15].

Among the wide range of cardiac abnormalities that are reflected in altered electrical behavior, we emphasize here two major categories: those resulting from obstructed blood flow to the coronary arteries (coronary heart disease, CHD) and those characterized by altered heart rhythms (arrhythmia). Heart disease remains the most frequent cause of death in the Western World—CHD produces some 1.5 million heart attacks annually, of which one third are fatal. Electrical effects of CHD are caused either by the imbalance of ionic concentrations due to acute obstructions or by the cell death that follows if treatment is too late or unsuccessful; in both cases AP shape and size are altered regionally, resulting in changes in the body-surface ECG [16]. Arrhythmias, which range from benign to deadly, arise from many causes, and are often very dynamic in nature. Classic features of the underlying electrophysiology include tissue which supports only very slow or directionally dependent propagation or spontaneously active pockets of tissue. Their dynamic nature and complex origins make many arrhythmias difficult to detect and problematic to treat [17].

In this section we will briefly describe some relevant cellular electrophysiology and the electromechanical link, some macroscopic characteristics of cardiac tissue that affect the spread of activation throughout the heart, and the relationship between intracellular activity, extracardiac potentials, and the body surface electrocardiogram.

2.1 Cellular electrophysiology and the electro-mechanical link

The human heart weighs some 300 g and is about the size of a large man's fist. The billions of muscle cells of which it consists are each capable of generating electric currents and potentials that are functions of ionic concentration differences across their membranes. In particular, the resting transmembrane potential difference of a cardiac cell (inside relative to outside) is negative, and depends largely on the ratio of the concentrations of ionic potassium ($[K^+]_i/[K^+]_o$) inside versus outside the cell. If the concentration gradient changes, the membrane potential does too. Induced changes in transmembrane potential can alter the permeability of the membrane, allowing ions to flow down existing concentration gradients and further altering the transmembrane potential—when the resulting feedback is positive, the consequence is a transient breakdown of the resting potential, or depolarization, and an action potential (AP). A cardiac AP consists (coarsely) of 1) a rapid (1–10 ms) activation phase during which the membrane depolarizes and even reverses polarity, 2) a much longer (200–350 ms) intermediate interval of relatively stable potential, known as the plateau phase, and 3) a relatively slow (100 ms) repolarization phase during which the transmembrane potential recovers to its resting value (see Figure 1).

Please place Figure 1 here

The following aspects of this process are critical to cardiac function:

1. The electrical currents and potential differences generated by one cell during depolarization can trigger depolarization of neighboring cells; thus a wavefront of depolarization, or activation, can propagate through cardiac tissue once some part of the heart depolarizes.

2. The transmembrane currents are carried by ion movement; one consequence of the ion movement responsible for depolarization is an increase in the concentration of intracellular calcium, which initiates a contraction of the cell. This is the basis for contraction of the entire heart.

3. After one depolarization, a second depolarization cannot take place until some degree of repolarization is complete. This necessary interval, known as the refractory period, ensures a minimum time interval between two muscle contractions.

Thus there is a tight link between the pattern of cardiac electrical activity and the mechanical functioning of the heart. A change or distortion in the electrical behavior may produce altered contractile behavior, while mechanical or chemical damage to the tissue may alter the electrical pattern (by mechanisms not described here). This is the primary reason that measuring the electrical activity of the heart is of interest from a diagnostic viewpoint; it is reasonable to presume that by measuring and interpreting cardiac electrical behavior we may learn about the state of the myocardium (heart muscle).

Modeling the spread of cardiac activation is extremely complicated and the subject of considerable contemporary research. (For a recent overview, see the review article [18].) From an electro-chemical viewpoint there are a large number of separate ionic currents and mechanisms to monitor and model; from a dynamical systems viewpoint the problem is one of three-dimensional propagation in a non-linear, excitable, attenuating medium with refractory behavior and a very complicated anisotropic geometry. Modeling techniques range from detailed descriptions of coupled membrane elements with separate dynamic permeabilities for numerous individual ion types (possibly several each), through more functionally oriented approaches based on non-linear differential equations that approximate membrane dynamics over larger space scales, all the way to cellular automata models. Since our focus here is on extracardiac potential measurements we will only mention that research into linking propagation models with extracardiac and even body surface potentials is in its infancy and promises to be an exciting area in the future.

2.2 Anatomy and cardiac electrophysiology

The human heart has four chambers; the upper chambers, the left and right atria, receive incoming blood from the lungs and the body respectively, while the lower chambers, the left and right ventricles, pump blood out to the systemic and pulmonary circulatory branches. When the heart beats normally, the depolarization wave that initiates the mechanical contraction starts at the top of the atrium from pacemaker cells and propagates through the atrial walls down to the interface with the ventricles. The atria and the ventricles are electrically insulated at this interface except for a region known as the atrial-ventricular (AV) node. The AV node acts like a delay line, retarding the activation signal for about 100 ms; this allows the atrial contraction to finish before the ventricular contraction begins. Once the signal clears the AV node it is carried along a specialized non-contractile conduction system, starting with the bundles of His, then proceeding very rapidly through a branching network known as the Purkinje Fibers, to numerous sites along the inner chambers of the ventricles. From there the depolarization wave spreads into the working myocardium, where it propagates from cell to cell outwards through the walls and upwards towards the base of the heart; this sequence coordinates the timing of the mechanical pumping so that the blood is squeezed upwards and outwards from the ventricles in an effective manner.

Cardiac tissue is highly anisotropic in its structure, with each ventricular cell having a size of approximately $200 \times 20 \times 20$ μm and electrical coupling between cells occuring preferentially—but not quite exclusively—at the narrow ends. Muscle striation also aligns with the anatomical structure so that cells always contract along their long dimension. The fiber orientation changes

dramatically throughout the heart—fiber direction rotates up to 120° in a few centimeters from outer to inner walls of the left ventricle [19]. One result of this fibrous structure and its consequent macroscopic electrical anisotropy is that the activation spreads three to five times faster along fibers than it does across them [20]. Thus initiation of activation at a point results in an elliptically shaped wavefront, whose axis rotates as a function of underlying rotation of the fiber direction [21]. Further complexity in propagation results from the interaction with the Purkinje system, which stimulates many regions of the heart almost simultaneously, resulting in a large number of micro-wavefronts that eventually merge into a highly complex set of macro-wavefronts.

2.3 Extracellular potentials

To investigate the behavior of even modest volumes of cardiac tissue requires electrodes located outside the individual cells. Such electrodes do not measure transmembrane potentials, but instead respond to extracellular potential differences between regions of the myocardium. Hence the shape of the waveforms they measure do not resemble APs. For example, during the activation phase, the region between resting and depolarized tissue forms a shell approximately 1 mm thick with an extracellular potential drop across it of 30–50 mV. function The movement of this activation wavefront past a recording electrode which is referenced to a distant "reference" electrode creates a rapid downstroke in the measured signal, referred to as the "intrinsic deflection", that is a characteristic feature of each electrogram (the name given to a waveform that is measured by an electrode placed on or within the myocardium).

If we move this electrode further and further away from the heart surface, it will sense a larger and larger volume of cardiac tissue, and the shape of the measured signal will change. One important effect is temporal smoothing, which is caused by spatial superposition rather than temporal dispersion. At the body surface, each electrode records what is now called an "electrocardiogram". The ECG waveform typically displays a trimodal (-/+/-) deflection (the "QRS complex") during activation, reflecting the approach, passage, and departure of the wavefront from the region of the heart to which the electrode is most sensitive. This is followed by a constant or slowly changing potential level corresponding to the AP plateau phase (the "ST segment"), and a smooth bump (the "T wave") which reflects recovery or cellular repolarization. The drawings in Figure 1 illustrate schematically the potentials sensed by a body surface electrode, an extracellular cardiac electrode, and the transmembrane potential in three different cells within the heart. Figure 2 shows the effect of spatial superposition in a simplified arrangement in which an isolated, perfused heart is suspended in a human shaped electrolytic tank (see Section 3.3 for more details). Both epicardial and tank surface potentials can be recorded simultaneously and their spatial complexity compared. Striking in the figure is the fact that several independent areas of positive and negative potential can be observed on the epicardium, while the torso reveals only a single positive and a single negative area. The difference in scaling of the maps also illustrates the attenuation that occurs from the heart to the body surface.

Please place Figure 2 here

We wish to emphasize that these waveshapes can vary dramatically depending on the location of the electrode with respect to the direction of the wavefront and to anatomical features (e.g. cardiac fiber orientation or position of the heart and internal organs) as illustrated in Figure 3. Part (a) of this figure shows four human electrocardiograms recorded simultaneously from various locations on a patient's torso; note the dramatically different shapes of QRS, the inverted (opposite polarity to the QRS) T wave in one location, and the variability in amplitude. Part (b) shows

four electrograms recorded simultaneously from the epicardium (the outer surface of the heart) of a dog using a 256 sensor (16x16) 3 cm square array; although all four waveforms show the clear negative-going intrinsic deflection, the shape (or even presence) of the R wave (positive-going deflection preceding the downstroke), the shape of the S wave (immediately after the downstroke), and the shape and relative size of the T wave, all vary significantly despite their spatial proximity. This figure also underscores that, although there is effectively no temporal superposition or filtering between the APs and the extracellular measurement point, the effect of *spatial* superposition is that the temporal behavior of the waveforms becomes progressively smoother (or more low frequency) as we move away from the heart.

Please place Figure 3 here

One feature of cardiac propagation that illustrates some of its unusual and non-linear behavior is the annihilation that occurs when two wavefronts meet. Instead of passing through each other, as many other classic propagating waves do (for instance, fluid, acoustic or electromagnetic waves), when one depolarization wavefront meets another, neither can propagate in their original direction because both will have reached regions of recently depolarized, and thus refractory, tissue. If, for example, two elliptical wavefronts moving towards each other from opposite directions collide, the overall effect will be a $\pi/2$ rotation in propagation directions. Another unique characteristic of cardiac activation is that there are several regions of tissue capable of spontaneous regular depolarization. However, due to the refractory effect, the most rapid-firing region is capable of suppressing the others. In what is known as "normal sinus rhythm" the pacemaker cells at the top of the right atrium dominate, but in some arrhythmias a region of ventricular tissue may take precedence over the normal sinus rhythm.

2.4 View from the body surface

From the preceding discussion, it is clear that the heart acts as a spatially and temporally distributed electrical source with complex dynamics, embedded in an irregularly shaped volume conductor with conductivity inhomogeneities. If we consider the view of the cardiac source seen from an electrode on the body surface, we therefore have to take into account

1. the distributed nature of the source potential patterns,

2. the presence of conductivity inhomogeneities (the internal organs) between the heart and body surfaces, some of which have significantly anisotropic conductivity,

3. superposition effects between the distributed source and any given location on the body surface; any particular electrode is sensitive to the activity of the entire heart at any given moment[1], with the relative influence of any given point on the heart determined by the effective current path between the two points. This effect depends only on the anatomy and conductivities in the torso volume conductor.

4. attenuation of signal strength due to dispersion as the currents pass through the intervening tissue.

[1]We note that linear and quasi-static approximations are valid here, given the tissue properties and frequency ranges involved. In particular there are no significant temporal dynamics in the volume conductor, and events on the heart can be treated as being seen instantaneously on the body surface. However, as noted earlier, the effect of spatial superposition can cause temporal as well as spatial smoothing of the body surface potentials with respect to epicardial potentials.

2.5 Strengths and limits of standard electrocardiography

Despite its simplicity, the standard ECG plays an important role in clinical medicine. From two electrodes one can measure heart rate and detect some heart rhythm abnormalities; as few as three electrodes may be adequate to determine, albeit coarsely, the location of cardiac ischemia (insufficient blood supply to the heart muscle) and infarction (heart attack), and from the full "12-lead ECG"—actually derived from 9 electrodes—cardiologists are capable of localizing some sites of aberrant conduction between atria and ventricles or areas of transient ischemia and even detecting the presence of physical abnormalities such as enlarged heart volumes or congenital structural heart defects [22]. However, the limits of the standard ECG are undisputed: events in the anterior region of the heart can be detected because of the proximity of electrodes on the chest wall but significant errors occur when events occur in other regions of the heart; features of the ECG such as deflection of the ST segment during ischemia may be underestimated if they happen to be weak or non-existent on the regions of the torso sampled by the leads; the ECG is the spatial integral of many simultaneous events, some of which partially cancel so that small defects can result in large changes in the signal, or vice-versa—hence the size of ECG change may not reflect the extent of physiological alterations.

Given the complexity of cardiac electric fields, it is not surprising that their interpretation is problematic, especially based on the standard ECG. The need for improved approaches motivated the methods described in the rest of this paper. In particular, better data acquisition capability enabled the development of cardiac mapping in response to the need for more information. As with other imaging methods, electrical mapping is an outgrowth of advanced electronic and computer technology, and just as standard X-rays are supplemented and sometimes supplanted by CT, the standard ECG should be enhanced by the development of cardiac electrical imaging.

3 Cardiac mapping as an imaging modality

3.1 Basics of cardiac mapping

The primary technique of cardiac mapping is to increase the number of sensors in order to recover a more complete picture of cardiac electrical activity. These maps can be recorded during invasive or experimental studies in which electrodes are inserted into the chambers of the heart [23], into the walls of the heart [24], or on the outer surface of the heart [25], or non-invasively from the surface of the body [5, 26]. The technology of mapping has evolved over the past thirty years from dual-trace oscilloscopes with cameras to acquisition systems capable of recording from 4000 channels at 1500 samples/s. The electrodes can be mounted in needles with contacts every 1-2 mm; linear arrays of wires with spacings in the range of 100 μm; inflatable balloons or flexible "basket" catheters; rigid, planar arrays or flexible nylon socks with hundreds of individual contacts; or strips of ECG electrodes spaced 1–10 cm apart. Mapping in most clinical settings serves either as an experimental tool, where the additional time and expense are justified by the need for detailed information, or in special cases, such as detecting complex arrhythmias that do not respond to conservative treatment [23]. The exception remains Japan, where body surface potential mapping (BSPM) has recently become common practice [27]. Some methods used to analyze maps are described in the next section.

A more contemporary approach to mapping is to view it as a *medical imaging modality*, *i.e.*, similar to computed tomography (CT), magnetic resonance (MRI), or ultrasonography. Electrical imaging has certain commonalities with other imaging modalities, and a few significant differences. Perhaps the most obvious difference, as mentioned earlier, is the goal: we seek to describe

or reconstruct the spatial and temporal distribution of electrical potentials and currents, and the organization of the underlying source mechanisms, rather than anatomy or tissue characteristics. Another major difference with many other imaging modalities is that this is a *passive* sensing method rather than an *active* one such as X-ray CT, MRI, or ultrasound; that is, we passively measure energy generated by the organism, rather than measuring the transmission or scattering of energy which we have actively injected into the organism. Finally, in contrast with electromagnetic and acoustic imaging, this is a *low-frequency, quasi-static* problem—this means that there is effectively no model for phase information available to aid the imaging process. Despite these differences, as with most imaging technologies, the basic problem is similar; we have available only a remote, distorted, blurred, and attenuated measurement of the process which we are seeking to characterize, we have multiple "views" of the this process from different "angles", and the medium between source and observation, which causes the blur and attenuation, is space-varying. Thus there are some formal similarities, for instance in the inverse problem described in Section 5, with other imaging and tomographic modalities.

3.2 Technical requirements of cardiac mapping

There are a number of technical requirements in cardiac imaging, some of which remain the topic of ongoing research. These issues include spatial and temporal sampling densities, the choice of reference potential, acquisition and modeling of a geometric substrate, and visualization of the images.

The most basic practical question in cardiac image acquisition is the number and location of electrodes used, both functions of spatial sampling density and electrode sensitivity. Although the discrete nature of the cellular source implies that there is information present at frequencies corresponding to the dimensions of a single cell, this is clearly not a practical sampling distance. Except for optical techniques relying on voltage sensitive dyes [14], the subject of intensive development but still restricted in their application, transmembrane potentials cannot be measured at more than few sites simultaneously with present microelectrode technology. Minimal extracellular electrode spacing ranges from sub-millimeter on the epicardial surface, to 5–10 mm between multi-electrode needles in the heart walls, to 10–30 mm between body surface electrodes. However, the underlying question, still without a clear answer, is what the tradeoffs are between expense and information gain as a function of sampling density. Limited studies have tried to address the issue in terms of spatial frequency content [28], but the problem is complicated by anisotropy, surface curvature, and irregular shape. On the heart surface, studies such as those in [25] suggest that details of wavefront breakthroughs at the surface and quantitative information about wavefront velocity, thickness of the wavefront, and potential gradient, are lost with spacing greater than 2 mm. In order to sample the entire epicardium simultaneously, this spacing would require an electrode array size which is impractical with current technology. Temporal sampling rates are easier to determine, although the rate chosen often depends on the application. The general ranges are from 250–1000 Hz. on the body surface, 1000–2000 Hz. for ventricular extracellular measurements, 5000–10,000 Hz. for transmembrane APs, and up to 15,000 Hz. for recordings in the specialized conduction system of the heart [29].

When recording extracellular potentials, either bipolar or unipolar electrodes can be used[2] In the former case local activity is accentuated at the cost of a more global image, and for both body surface and direct cardiac mapping the latter choice is more common. However with unipolar electrodes there is no clear "ground-truth" reference; usually either a mean potential over the

[2]With bipolar electrodes each measured signal is the potential difference between two closely spaced electrodes, while with unipolar electrodes all signals are referenced to the same common potential.

surface or the "Wilson Central Terminal" (the mean of left and right arm and right leg potentials) is used. Taccardi *et al.* have recently shown that neither of these references is constant in time, which may prove to have important consequences for interpretation of electrical image sequences. [30]

The generally irregular spatial sampling, often over a complex surface or volume, is one feature which differentiates cardiac electrical images from most common medical images modalities. Both for image display and for modeling of source/measurement relationships (see Section 5), a record of the electrode locations is needed, in addition to the samples of potential data itself. This provides a geometric substrate upon which the potential data sit. The geometric information can be acquired either through digitization of a particular electrode arrangement (often via an anatomical imaging modality) or the use of a standardized electrode placement scheme.

Finally, since fully automatic algorithms to interpret and process these images are still being developed, investigators need adequate visualization tools to evaluate and understand the data and their results. Of particular difficulty is visualization of data in two or three dimensions acquired on an irregular sampling grid as described above. Either the data is interpolated to a regular grid and standard techniques are used, with obvious consequences in terms of smoothing and increased data volume, or the interpolation is performed directly on the irregular grid. The latter approach requires customized interpolation algorithms and software[31, 32]. Moreover, given the spatial and temporal complexity of the data, animation and interactive manipulation of the geometry and the potentials are usually essential. Finally, the use of pseudo-color mapping greatly enhances interpretability, and flexible control over such mapping schemes is an extremely useful feature of visualization software for electrical image display and research.

Figures 4– 6 show visualizations of sequences of isopotential maps recorded under three different conditions. In Figure 4 the recording array contained a closely spaced (2 mm) regular grid (25×21) of silver wires that were placed on the epicardial surface of an exposed dog heart. The sequence shows isopotential contour maps from four instants in time from the same beat (marked by the vertical line in the time signal below each map) stimulated from a single ventricular site near the center of the array. The cost of this spatial detail lies in the fact that within 40 ms the activation wavefront has moved almost entirely off the edges of the array. Also shown are two maps derived from the complete sequence of potential images. These "activation time" and "recovery time" maps are described in more detail in Section 4.1.2.

Figure 5 also contains epicardial potentials, but recorded from a 490-electrode sock that surrounded the ventricles and thus had a much coarser spacing than the grid in the previous figure. Here five instants from the initial 70 ms after stimulus from a single ventricular site, and one from the peak of the T wave, are shown, but with much less spatial resolution than with the fine grid array. The advantage of this arrangement is that the entire heart is covered so that large scale phenomena can be observed. Figure 6 contains a sequence of isopotential maps from a human subject, recorded with 117 electrodes placed in an irregular array over the entire thorax. The pattern is spatially much less complex than those seen in the previous figures, an effect of the superposition described in Section 2.3 with a few dominant features visible. However, the temporal course of the map sequence is more rapid than in the previous examples because normal cardiac activation does not occur from a single site, but from a large number almost simultaneously, the result of the specialized conduction system described in 2.2.

Please place Figure 4 here

Please place Figure 5 here

Please place Figure 6 here

3.3 Experimental mapping studies with electrolytic tanks

One difficulty confronting investigators who want to evaluate the information content of electrical images is obtaining data under controlled conditions where the "true" information is known. This is particularly true when the goal of the method is to determine the state of the heart from recordings made from the body surface. An indirect solution, using data acquired during clinical procedures where controlled changes are introduced, is limited in extent and applicability. Some surgeries permit images to be acquired from the exposed heart surface but these are not representative of the potential distributions that occur when the chest is closed, because the exposed heart surface is in contact with an insulator (air)—thus current paths change, and as a result so do potential distributions. Surgically instrumenting animal hearts and then closing the chest cavity is another approach [33], but it is expensive and is hindered by the technical difficulties of maintaining access to an adequate number of electrodes in the heart and by the need to allow some days or even weeks for the animal's torso to regain its original integrity. In humans, it is clinically appropriate in some situations to leave a few cardiac leads in place for the purpose of post-operative monitoring or pacing, but the limited number of such leads preclude any serious mapping efforts.

Therefore researchers have developed physical models of the thorax from which direct measurements are possible. Realized initially in two dimensions with conductive paper and shortly thereafter as torso-shaped electrolytic tanks [34], early versions included discrete current bipoles as sources. Their primary application was to evaluate the theory of electrocardiographic lead placement and sensitivity under the assumption of a dipole equivalent source. Later studies included pairs of dipoles [35] and then perfused, isolated animal hearts [36, 37] in cylindrical tanks. The most recent electrolytic tanks are shaped like a human torso, contain electrodes mounted in the tank surface and may use movable electrodes to probe the volume potentials [38, 39, 40, 41]. The sources are typically isolated animal hearts that are instrumented with epicardial sock arrays, cages, and/or transmural multi-electrode needles. Figures 2 and 5 contain measurements from such a torso tank.

In the context of electrocardiographic imaging, torso tanks serve the same purpose as the phantoms commonly used in other scanning modalities to evaluate the accuracy and capabilities of the system. They are especially useful in providing data with which to examine the effects of abnormalities such as ischemia (which can be induced by manually constricting cardiac arteries), and to validate forward and inverse solutions, and examine their sensitivity to errors in the geometry and conductivity of the torso.

4 Electrical Image Sequence Representations

Because of the volume of data and the difficulty of distinguishing and (especially) quantifying important features, a number of techniques have been used to represent, display, and compress electrical image sequences. Here we present an overview of some of the most successful and/or promising. We have attempted to classify the techniques into two categories, those based directly on representations of the data as a "map" and those based on representing the data as an alternate set of features or coefficients extracted by means of transform techniques and/or statistical analysis.

4.1 Potential Mapping and its Direct Descendants

The most straightforward presentation is to use interpolation and contouring to create potential maps, presented as contours or shadings of constant potential (isopotentials), separately for each

image in a sequence. Required processing includes interpolation, contour generation, and color mapping and scaling. Although this representation gives a literal picture of the sequence of potential distributions, it does little to clarify the complexity of the data and nothing to reduce their volume. Experts can interpret these maps, and differences between them, to extract a great deal of information, but automatic and/or objective processing is difficult. In addition, there are some subtle ambiguities and limitations in isopotential mapping as a representation which have helped motivate the development of more sophisticated techniques:

- Isopotential maps interpolate in space but not in time. Thus a smoothness is imposed on the spatial distributions based on the chosen interpolation technique, but not on the temporal progression; this may cause misinterpretation of the suddenness of temporal events, and likewise may mask events with high spatial gradients.

- To minimize the computational complexity, the spatial interpolation is usually done via bilinear bases in two dimensions (or trilinear bases in three dimensions). This may cause considerable distortion, for instance during activation, when there is a strongly non-linear distribution of potential with space across the wavefront [42, 43]. In addition, there is an inherent ambiguity at saddle points when linear interpolants are used, which means that alternate triangularizations can produce quite different contours [44].

- Isopotential maps are often drawn using different line types, color ranges, or symbols, to distinguish between regions of positive and negative potential. The visual effect is to accentuate the location of the zero-potential contour. While this contour often lies in regions of sharp gradient between maxima and minima, it is really the latter which have direct biophysical meaning, while the significance of the former is unclear because there is no absolute reference against which the potentials are measured. In fact the reference used in practice may not be constant in time [30]. Nonetheless, practioners often assign great value to the location of the "zero-line" as a topographical feature in isopotential maps [45].

- Contouring for isopotential maps can be quite sensitive to errors in electrode position and the spatial resolution of the sensor array, dramatically changing the shape of a contour line with a small change in electrode location or measured value [46].

- Isopotential map sequences are notoriously difficult to quantify. Common difference measures include RMS-type ($\ell 2$) errors, which are well known to be poor measures for images; correlation coefficients, which are insensitive to amplitude differences; and descriptive features, which are hard to objectify. In addition, when comparing two beats it is necessary to align them in time. This alignment can also be ambiguous due to the lack of temporal interpolation and the difficulty in choosing a unique alignment instant between two signals that may differ significantly.

Despite the limitations of isopotential maps, they have one primary advantage: by leaving the interpretation in the eye of the human observer, they take advantage of our ability to interpolate in time and space, extract edges, *etc.*, and thus to "see" wavefronts and other coherent events as distinct from the background. In an attempt to reduce the data volume and concentrate the information in maps, there have been a number of other mapping techniques developed; we describe two of them below.

4.1.1 Isointegral Mapping

In this technique, the signal from each lead is integrated over time, producing a cumulative temporal potential at each spatial location. The end points of the integration are determined by either visual or algorithmic analysis of the morphology of the waveforms. Different temporal periods, *e.g.* QRS, the ST segment, QRST, or even subintervals of QRS or the ST segment, are often integrated separately, and the results presented in iso-integral contour maps. When intervals of different absolute length are to be compared (for instance from beats of different duration) the map sequences are sometimes interpolated to a common number of samples or the integrals are normalized by their length.

Integral maps achieve a great deal of data compression, but at the cost of information loss, and in addition have several technical problems. In addition to contouring, this technique requires the determination of temporal "fiducial points" to segment the heartbeat. (Although somewhat outside the scope of this paper, we note that this process is fairly robust when applied to an RMS signal over an entire image to find globally defined fiducials, but may suffer from considerable error—and is a subject of current research—when applied to each lead individually [47].) The advantages of integration include a dramatic reduction in data volume, considerable robustness to mis-alignment of different beats (although perhaps not to integration endpoints), and some possibility of direct physiological interpretation of the resulting maps, especially the QRST integral [48, 49, 50].

4.1.2 Isochrone Mapping

One feature of great physiological interest in data recorded directly from the heart is the time at which each area of the heart depolarizes (known as the *activation time*), since the progression of this depolarization wavefront determines the contraction pattern. Activation time is calculated for each sensor by estimating the timing of the intrinsic deflection described in Section 2.3 (usually as the maximum negative temporal derivative). Thus an entire beat is reduced to a single isochrone contour map showing lines of interpolated equal activation times. This technique is generally used only on or within the heart, where the concept of the passage of a wavefront is well defined. It requires the detection of activation instants from measured time signals, a non-trivial problem when the signals have complex morphologies [51], which occurs frequently when the tissue is injured. A similar technique has also been used to determine "repolarization time", usually defined as the maximum positive derivative in the vicinity of the T wave. From these two instants the time between activation and repolarization, known as the Activation-Recovery Interval (ARI), can be calculated. The ARI is used as a measure of local recovery characteristics and is highly correlated with AP duration as measured from the transmembrane potential [52]. Examples of both activation and recovery maps are shown in Figure 4, together with isopotential maps from the same beat.

4.1.3 Difference Maps

"Difference mapping" is a commonly used technique to detect changes in cardiac state; images recorded under one condition are subtracted from those recorded under a control condition (similar to Digital Subtraction Angiography). For instance, there have been a number of research studies using data recorded during percutaneous transluminal coronary angioplasty (PTCA) procedures, when a balloon at the tip of a catheter is inflated in a coronary artery to open partial obstructions [53]. PTCA studies are good models for research on the electrical effects of ischemia; while the balloon is inflated, the tissue downstream from the inflation is effectively cut off from its normal blood supply and thus rendered ischemic. When the balloon is deflated, the tissue is reperfused.

Thus electrical image data can be recorded during PTCA with the chest closed (*i.e.* relatively non-invasively) and the electrical behavior of acutely ischemic and control episodes can be compared by computing difference maps. However, timing sensitivity is often too great to use differences of the image sequences themselves, so more commonly integral maps are first computed separately for each recording, and then "integral difference maps" are computed to reflect the integrated changes due to the ischemia-producing intervention. Figure 9 in section 5 contains examples of integral maps and an integral difference map calculated from recordings made during a PTCA inflation.

4.2 Feature/Coefficient/Basis-Vector Representations

In this section we describe a number of techniques which have been applied for representation of cardiac electrical image sequences. Some of the methods employ classical statistical techniques, while others use basis representations with complex exponential or wavelet bases.

4.2.1 Karhunen-Loeve Transform (KLT)

The most widely used transform technique for representing electrical image sequences, especially BSPM, is the KLT. It has been employed in a fashion similar to the way it is used for representation, compression, and feature quantification and pattern recognition for general digital images [54]. First the eigendecomposition is found of an empirical spatial covariance matrix; this matrix can be estimated from an image sequence corresponding to a single beat or from a large training database. (Here each image (time sample) is represented as a single vector via some reasonable ordering.) Individual time samples are then projected onto the eigenvectors to produce a multichannel time series of spatial KL coefficients. Only the components corresponding to the largest eigenvalues are retained (usually only about 12-20 out of around 200 are needed for good fidelity), forming a reduced-dimensional multichannel time series of coefficients. These coefficients can then be further compressed by taking advantage of the *temporal* redundancy; the *temporal* correlation matrix of the coefficients which have been retained is estimated and used to repeat the KL process along the time axis. Compression ratios up to 320:1 have been obtained with good accuracy [55, 56]. The spatial eigenvectors retained can be considered as representative of the most "typical" distribution patterns in the data and have been used to extract features (the KL coefficients for a particular image sequence) for classification algorithms [7, 57, 58]. This method requires a training database, and relies for accuracy on the extent to which this database represents a particular set of image sequences. It also relies on the assumption that the geometry of the sensor array is constant across the recordings in the training database as well as the recording to be transformed; this can be particularly difficult with direct epicardial recordings.

Figure 7 contains an example of spatial eigenmaps computed from the same single beat shown in Figure 4. The upper two rows of the figure contain the eigenmaps corresponding to the first four eigenvectors. The lower two rows contain reconstructions of isopotential maps for two of the time instants shown in Figure 4 (maps 1 and 4, at 10 and 261 ms, correspond to the third and fourth rows of the figure, respectively). The left map of each row was reconstructed using only the 4 eigenmaps shown in the top half of the figure, while the second reconstruction used the first 12—the 12 largest eigenvalues accounted for more than 99.5% of the energy of the sequence (which corresponded roughly to the signal to noise ratio). The isopotential map from late in the beat (261 ms) shows a much smoother distribution and is very similar to the first eigenmap; as a result, it is adequately reconstructed with just 4 eigenmaps. The distribution at 10 ms has more spatial detail and even with 12 eigenmaps the reconstruction still differs from the original.

Please place Figure 7 here

4.2.2 Best Lead Methods

Another way to represent cardiac electrical images in a statistical sense is through selecting the "best leads" to represent a particular database, either by KLT [54, 59] or discriminant [58] techniques. Both methods have been applied to select a relatively small number of leads (6-25) which contain most of the statistically relevant information in a particular data set. The accuracy of these methods tends to depend sensitively on exactly which leads are used, and the lead sets change significantly when different abnormalities are represented in the training data or are used to design the discriminant. In addition, direct information about spatial phenomena is lost in the resulting set of scalar leads.

4.2.3 Multi-Dimensional Power Spectra (Isopower Mapping)

Since activation and recovery are in some sense wavefront phenomena, classical signal processing techniques for sampled wavefield data have been applied to cardiac mapping. There have been several reports of using correlation-based and coherence-based approaches [60, 61]; here we describe a frequency-domain estimation method. Since the temporal signals are relatively wide-band (compared to pure tones), standard narrow-band array processing techniques are inappropriate. Investigators have used a wide-band array processing algorithm, the Zero-Delay Wavenumber Spectrum (ZDWS). The ZDWS is derived from the multi-dimensional (MD) frequency-wavenumber spectral estimate (FWSE) of the data, an estimate of the MD Fourier Transform of the correlation sequence of the data with respect to both space and time; its arguments are temporal and spatial frequencies, or alternatively temporal frequency and spatial wavenumbers. The ZDWS is computed by averaging the FWSE over temporal frequencies [46] and provides an estimate of the power of wavefront arrivals on the array as a function of wavenumber.

For a 2D sensor array, the results can be displayed as contour lines of equal power versus the two components of the wavenumber vector. Once peaks in this map are located, temporal frequencies at the peak can be estimated to give a measure of conduction velocity. Each beat is reduced to one image and the results have a direct physical interpretation, although temporal and spatial localization are lost over the array. Moreover, the ZDWS technique involves a number of hidden assumptions (far-field point source, plane waves, and a linear relationship between velocity and temporal frequency, for instance) which are not valid in cardiac tissue. This technique has been used with some success to distinguish ischemic from normal conditions [46] and to characterize frequencies in ventricular fibrillation [62].

4.2.4 Multichannel Temporal Power Spectra

Rather than use MD techniques, if spatial localization is desired, the array data can be treated as a multichannel sequence and the auto- and cross-spectra of the sensor data can be computed. This technique reveals temporal frequency domain behavior on a sensor-by-sensor basis. For the most part researchers have concentrated only on the auto-spectra. Reported use of such multichannel spectral estimates include the derivation of frequency domain detection statistics to discriminate healthy from injured tissue in epicardial [63] and body surface potentials [64], characterization of epicardial and surface potentials in tank studies [65], and the formulation of new solutions to the electrocardiographic inverse problem [66].

4.2.5 Wavelet Transform

Recently, a compromise among some of the difficulties of the previous methods has been attempted using the Wavelet Transform (WT)[67, 68, 69, 70, 71]. The WT has been used for spatial, temporal, and temporo-spatial transformations, and offers some new handles on tradeoffs between 1) sensitivity to temporal alignment when comparing instant maps from two different beats, 2) temporal resolution versus temporal stability, in a more graded fashion than that achieved by integral maps, and 3) the optimality of the KL transform versus its need for signal-dependent basis vectors. In addition the WT is *localizable*, offering the promise of sensitivity to local events in space and/or time and therefore of amenity to physiological interpretation (in contrast to, say, the KL or Fourier-based transforms). Contour maps made from the scaling function coefficients provide a controlled amount of smoothing and retain a known degree of temporal resolution. In addition, contour maps of the wavelet coefficients may reveal additional information not available in integral maps. Wavelets and Best-Basis techniques have been applied to segment BSPM sensor signals and plaque sensor signals automatically [47] and to locate activation and repolarization wavefronts on the epicardium in space and time [72].

5 Inverse Solutions

5.1 Introduction: the inverse problem of electrocardiography

Probably the most important goal in cardiac electrical imaging is to maximize the information about cardiac electrical activity which can be extracted from non-invasive measurements on the body surface. However, a significant part of this information is lost to attenuation and superposition in the torso volume conductor and cannot be recovered by processing body surface potentials directly, no matter how sophisticated the processing techniques. For this reason, there has been a great deal of interest for many years in both constructing a model of the torso volume conductor to calculate body surface potentials using realistic heart-torso models, known as solving the forward problem of electrocardiography, and then in using this forward solution, along with measured body surface potentials, to solve the associated inverse problem—to estimate epicardial potentials or other characterizations of the heart's electrical activity. In effect, the idea is to use the additional information incorporated into the forward model to at least in part reproduce what we could have measured, had we been able to move the sensors close to the heart surface or into the myocardium.

One can decompose the complete forward/inverse problem into a set of interrelated partial forward/inverse problems: between transmembrane potentials, propagation models, and electrograms; between potentials on the epicardium or a cardiac source model within the heart and the body surface; and between potentials on the inner walls of the heart (the endocardium) and electrodes inside the chambers. Of these, only the intracavitary/endocardial and cardiac source/body surface problems have received much attention in the literature. We concentrate on the latter problem here; for the former the reader is referred to [73].

Approaches to solving this problem have been based on two alternative formulations. The first employs a parametric model of cardiac sources, in which case the problem becomes one of source localization and parameter estimation. The second employs a non-parametric, distributed equivalent source model, typically characterizing cardiac sources by their reflection on the heart surface (epicardium and/or endocardium). This latter formulation leads to an image restoration problem; from a blurred, degraded electrical image measured on the body surface one attempts to use knowledge of the blurring function, *i.e.* the forward solution, to restore the "original image", the image one would have measured on the heart surface. In pursuit of the former approach to

the inverse solution, a number of parametric source models have been employed, among them single fixed or moving dipoles, multipoles, and uniform or non-uniform moving dipole layers (for a review see [74]). Although these have yielded some useful results, the lack of uniqueness (from Gauss' Law we know that only potential distributions on surfaces enclosing the sources are uniquely characterized by external measurements) and the complexity of the behavior one is trying to model (as described earlier in this paper) have led most investigators to use the second approach. (See [74, 75, 76] for a more detailed discussion of the tradeoffs involved in the choice of source configurations in inverse solutions.)

Even using this distributed, non-parametric, approach, there are two major alternatives. One can describe the equivalent source only in terms of activation time on the endocardial and epicardial surfaces; thus the problem is posed in terms of reconstructing an isochrone map from body surface potentials. Alternatively one can attempt a full reconstruction of the epicardial potential distribution. The advantage of the isochrone characterization is the reduction to a smaller number of unknowns which one is attempting to find—and thus the possibility of a better-posed problem—while still maintaining what is in some regards the most physiologically important feature of the solution; the advantage of the second approach is the retention of a complete description of not just activation but also repolarization and, generally, the distribution of potentials throughout the cycle. In the rest of this section we will concentrate on the epicardial potential/body surface potential formulation; it is still the most common model used in the literature, is the closest to image restoration problems which are more familiar to signal processors, and shares many major characteristics with other formulations. Where appropriate below, we will, however, refer to some of the work that has been reported for activation/isochrone inverse solutions.

5.2 The forward problem: principles and open questions

The forward solution for an epicardial potential source model is based on the solution of Laplace's equation in the source-free volume between the heart and body surface. Required elements of a solution are a geometric model that includes both surfaces and perhaps intermediate surfaces or the intervening volume, along with the electrical conductivity inside the enclosed volume. Construction of such a model requires acquisition of individualized anatomical information, usually by CT or MRI. The resulting images must be discretized and segmented, [77], the electrode locations mapped to the geometry, and the anatomical structures represented as a set of nodes in space which are linked into a mesh of polygons—triangles for surface descriptions and tetra- or hexahedrons for volume models [78]. This process is generally not yet fully automatic (and is a topic of research in many engineering domains). Conductivity varies locally within the thorax, causing local changes in field strength; however, the importance of such effects on the inverse solution has not been conclusively determined. Any internal organs that are included in the model are usually assumed to have piecewise homogeneous, perhaps anisotropic, conductivity. The geometry is treated as being static in time (in practice, of course, this is not the case but errors introduced by this approximation are considerably smaller than those caused by other necessary approximations [79]), and thus the forward problem needs to be solved only once for all time instants. Loading effects of the volume conductor on the source are also ignored, although recent experimental evidence suggests this may not be an accurate assumption [40]. The boundary conditions for the forward solution are the known potentials (or activation times) on the heart surface, continuity of the voltage and the normal component of the current across surfaces of internal inhomogeneities, and the insulated surface (zero normal current) condition on the body surface.

While analytic solutions to the forward problem are possible with simple geometries such as concentric or eccentric spheres [80], most authors have concentrated on the more practical approach

of using realistic geometries, defined as a mesh of connected nodes. Specific solution approaches include either writing volume integral equations from quasi-static versions of Maxwell's equations, or applying Green's Theorem surface integral equations, with appropriate boundary conditions, to all surfaces in the geometry. The resulting integral equations are discretized at the nodes of the geometric mesh and solved using standard techniques such as finite element methods (FEM) with volume equations or boundary element methods (BEM) for surface equations [80]. Finite element solutions can predict potentials anywhere inside the modeled volume, and can handle anisotropic conductivities (which are characteristic, for instance, of skeletal muscle), while boundary elements are simpler but only calculate the surface potentials and have more difficulty with anisotropy. Creating the required volume mesh for FEM is much more complicated than the surface meshes needed in BEM, and the matrices involved are much larger, although they are sparse, while BEM matrices are not. A combined finite-element/boundary-element method was described in [81] and recently significantly refined in [82].

If one stacks all the epicardial potentials at a particular time instant into a vector, and does likewise with the body surface potentials, the resulting forward solution is a matrix; the ith row can be thought of as a set of path weights, where each ijth weight relates the jth point on the epicardial surface to the ith point on the torso, or equivalently as the (index-reversed) impulse response of the ith spatial filter, whose input is the epicardial potential distribution and whose output is the ith body surface potential.

Early experimental studies of the accuracy of forward solutions left many unanswered questions. Primary among them were which internal organs (inhomogeneities) are important to include and how sensitive results are to accuracy of the mesh and the conductivity assumptions. Some recent simulation studies [39, 83, 84] and experimental results [40, 41] on these topics exist, but these matters are still largely unresolved.

5.3 The inverse problem of electrocardiography and image reconstruction

Since the effect of the volume conductor on the epicardial "image" can be seen as a space-varying spatial filter, from an image processing viewpoint the inverse problem is one of deblurring, or restoring, the epicardial image, given an observed blurred image and a known blurring function. In other words, we desire to reconstruct an *electrical* image of an internal organ from a number of smoothed external views. Thus the problem has both similarities and differences with both reconstruction and tomography problems found in the image processing literature, and there is considerable methodological overlap.

- The inverse problem is ill-posed, due to the smoothing and attenuating properties of the torso volume conductor. Hence, any discrete forward solution will produce an ill-conditioned forward transfer matrix. Straight-forward, unconstrained inversions will produce unstable results, such that very small perturbations in the data will cause unbounded (or unrealistic) oscillations in the inverse estimate. To illustrate the ill-conditioning problem, in Figure 8 we show the singular value spectrum for two typical forward matrices. From a filtering perspective, the forward filters are generally low-pass; thus the inverse filters must be high-pass, and therefore will be unstable to high spatial frequencies in the measurements. This is similar to what often occurs with blurred images, where the blur is a low-pass function.

- Although the forward filter is space-varying, a diminishing gain is achieved as one takes more spatial samples; this is reflected in the fact that including more and more points tends to produce forward matrices that are more and more badly conditioned. Again this parallels the typical image deblurring problem when the blur is space-varying.

- Image restoration methods are often dominated by the computational complexity involved, given the tremendous size (in pixels) of a typical digital image; here there is a considerable range in the dimensions, anywhere from 100–1000 points on the epicardium and 200–5000 on the torso surface. In general, however, the resulting forward matrices are much smaller than those that arise in standard imaging applications, where even a small image may contain 256 by 256 pixels and thus lead to matrices of some $(65{,}000)^2$ elements. Thus inverse methods which would be infeasible for digital image restoration may be feasible here, and methods which are essential for certain image restoration problems may not be as immediately attractive for this inverse problem—for example, iterative techniques are much less developed in this application than in image restoration.

- In image processing it is usually valid to assume regular spatial sampling of a flat (2-D) object on a square grid; here the surfaces are not flat and the sampling is unlikely to be either regular or square. Thus solutions which depend on the sampling assumptions (for instance, using Fourier Transforms) either do not apply or require significant modification.

- In some tomography problems, there is phase information in the measurements because the wavelengths are small compared to the physical problem size. As mentioned earlier, here the wavelengths are much larger than the problem size, low-frequency quasi-static approximations are valid, and there is essentially no phase information to aid in the reconstruction in the usual tomographic sense.

- As we will discuss below, stabilizing solutions against the ill-posedness of the inverse problem requires the imposition of *a priori* knowledge or assumptions about solution characteristics. The types of assumptions which best characterize images (for instance, Gauss-Markov random field assumptions) are unlikely to characterize cardiac electrical images, and likewise the types of structures and patterns likely to be present in electrical images will seldom appear in natural or man-made digital images. One consequence is that inverse solutions have been primarily formulated as deterministic, with few attempts to apply statistical models as is common in image restoration problems.

- Although the forward problem is quasi-static, there is a temporal correlation between nearby time samples of each lead, and an even stronger spatio-temporal correlation between the images on either the epicardium or the body surface; the wavefront behavior of cardiac electrical activity means that epicardial potential distribution patterns "move" coherently across the surface, at least over small spatial regions and time intervals. The biophysics of the forward problem ensure that body surface potential distributions are a smoother, remote reflection of the same behavior. Thus temporally uncorrelated behavior in an inverse solution is likely to be an artifact of the reconstruction. This temporal dimension has been used to aid inverse solutions, either explicitly [85, 86, 87, 88] or implicitly [89, 90, 91, 92]. Although there is currently considerable interest in temporal and spatio-temporal processing of digital image sequences, particularly in coding applications, there has been little use of temporal information in restoration problems.

Please place Figure 8 here

5.4 Solutions to the inverse problem

To stabilize inverse solutions against this sensitivity to small perturbations in the data or inaccuracies in the forward model, additional constraints, based on *a priori* additional information, must

be imposed on the solution. Straightforward least-squares solutions will not give reliable results due to the presence of the reciprocals of the small singular values in the inverse, and even truncated SVD solutions are not very effective because of the lack of a clear distinction between "significant" and "insignificant" singular values (see Fig. 8). The most common approach to this problem has been to use a technique known as regularization—the least-squares residual error cost function is supplemented by a second term which penalizes for large values of a chosen property of the solution [93, 94]. Thus a tradeoff is constructed between fidelity to the data (small residual error) and fidelity to the constraint represented by the second term (small regularization error). This tradeoff is controlled by a multiplicative weight known as the regularization parameter.

To illustrate more precisely how regularization works in a specific formulation, assume we have a forward matrix $\mathbf{A}$ and a measured torso data vector $\mathbf{y}$ at a particular time instant, and we wish to estimate a vector of epicardial potentials $\mathbf{h}$. Then, using the 2-norm of the estimate as a regularizer (a very common choice in practice), we can write the regularized cost function as:

$$\hat{\mathbf{h}}_\lambda = \arg\min_{\mathbf{x}} \left(\|\mathbf{y} - \mathbf{A}\mathbf{x}\|^2 + \lambda^2 \|\mathbf{x}\|^2 \right), \tag{1}$$

where λ^2 is the regularization parameter.

If we write $\mathbf{A}$ in terms of its SVD, $\mathbf{A} = \mathbf{U}\mathbf{\Sigma}\mathbf{V}^T = \sum_{i=1}^{r} \sigma_i \mathbf{u}_i \mathbf{v}_i^T$, where $\mathbf{U}$ and $\mathbf{V}$ are orthogonal, $\mathbf{\Sigma}$ is $\mathrm{diag}(\sigma_1, \sigma_2, \ldots, \sigma_r)$, the σ_i are the singular values of $\mathbf{A}$, ordered in non-increasing fashion, the $\mathbf{u}_i(\mathbf{v}_i)$ are the rows of $\mathbf{U}(\mathbf{V})$, and r is the rank of $\mathbf{A}$, then the solution to equation (1) can be written as [93]

$$\begin{aligned} \hat{\mathbf{h}}_\lambda &= (\mathbf{A}^T\mathbf{A} + \lambda^2\mathbf{I})^{-1}\mathbf{A}^T\mathbf{y} \\ &= \sum_{i=1}^{r} \left(\frac{\sigma_i}{\sigma_i^2 + \lambda^2} \right) \mathbf{v}_i \mathbf{u}_i^T \mathbf{y}. \end{aligned}$$

From this equation we can see that for those terms in the sum for which $\sigma_i << \lambda$, the λ^2 in the denominator acts to overcome the destabilizing effect of these small singular values. Thus the term in parenthesis represents a kind of filter to combat the ill-condition of the forward matrix. Similar results can be derived for more general regulariation scenarios.

There are three key questions in applying regularization techniques:

1. how best to choose the appropriate regularizer, *i.e.* the constraint,
2. how best to choose the regularization parameter, and
3. how to define "best" in the first two questions.

The most common approach to the first question has been to choose constraints which are both easily tractable and physically reasonable—in particular the energy ($\ell 2$ norm) of the result or of an estimate of its spatial gradient or Laplacian. Numerous techniques have been proposed to answer the second question [93, 95]; there are both *a priori* techniques based on assumptions about noise, model error, and correlation structure of the solution, and *a posteriori* techniques which first compute results for a (generally large) number of potential regularization parameters and then choose the best according to some criterion. Unfortunately, the results tend to be extremely sensitive to the interrelationship between the value chosen for the regularization parameter and the amount of perturbation or noise in the data. Little attention has been paid to the third question in the literature: generally $\ell 2$ norms are used in the cost functions and results are evaluated in terms of relative squared error, correlation coefficients, and visual interpretation, as described in

Section 4.1. The development of better measures of difference between electrical image sequences remains a question for future research.

Regularized solutions to the inverse problem of electrocardiography first appeared in the mid-70's [96]. Since then considerable effort has been put into finding more reliable and controllable inverse solutions. Initially much of this effort went towards studying the effects of various regularization constraints and the choice of the regularization parameter [38, 97, 98, 99]. More recently a number of more elaborate approaches have been developed, concentrating on new, decomposed, or combined regularization constraints [85, 86, 87, 88, 90, 100]. Such solutions have been used to localize specific abnormalities in the activation pattern [101], but so far have not been able to adequately and reliably reconstruct the general epicardial potential distribution. Nevertheless, in particular cases, inverse epicardial solutions do reveal details of the epicardial distribution that are not evident with other methodologies such as integral difference maps or singal instant potential maps. In Figure 9 computed inverse solutions are compared to integral difference mapping of the body surface data. Both parts of the figure shows maps from beats recorded just prior ("*pre*") to PTCA balloon inflation (A) and during the last 15 s ("*peak*") of the inflation (B), as described in Section 4.1.3. The upper panel contains iso-integral maps from both beats and their difference, ($peak - pre$). The lower panel shows both *measured* torso potentials and *inverse computed* epicardial potentials for one time instant during both beats.

The expected hemodynamic effect of balloon inflation is to induce local ischemia in tissue which is downstream from the site; electrically, the effect should be a change in local membrane resting potentials, with resulting shifts in the epicardial and torso surface potential distributions. The figure shows this as more positive (color shift from dark blue towards red in the figures) potentials on the anterior surface of the torso in both integral and instant maps. The inverse solution predicts more specifically the site of epicardial potential elevation which, in fact, corresponds qualitatively quite well with the region downstream from the location of the PTCA balloon (marked with the arrow in the figure).

Please place Figure 9 here

Among the areas of recent development have been the incorporation of more constraints, and especially of temporal constraints in addition to spatial constraints. Some example temporal constraints include ensuring that the temporal frequency content of the reconstructed signals is generally low-pass [85, 86], or that there is a sharp temporal gradient in the signal at activation time [91]. Another approach proposed recently is to apply regularization not to the entire forward solution matrix, but only those regions that display considerable levels of ill-conditioning [100]. Solutions have also been proposed using entropy criteria to reconstruct the multi-channel power spectrum of the epicardial signals [66]. Some recent approaches avoid the need for regularization, either by restricting the search to breakthroughs, modeled as independent sources, and found using subspace based techniques [102], or by posing the problem in a set-theoretic admissible solution framework and using convex optimization techniques [103]. The latter approach is similar in spirit to work that has been done in image restoration [104].

6 Concluding Remarks

In this overview we have described the contemporary state of a non-traditional medical imaging modality whose ancestry reaches into the last century, to origins in string galvanometry and the most rudimentary notions of bioelectricity. Electrocardiographic imaging addresses the limitations in spatial sampling and information extraction of the standard ECG by acquiring a much richer

data field, and then applying sophisticated signal processing and analysis techniques in order to extract more information from this data.

The overriding rationale for developing an electrical sensing methodology for the heart is the electromechanical link, which we have described in some depth. All mechanical events in the heart connected to its contraction and pumping function are preceded and controlled by electrochemical events; the latter also generate ionic currents, and thus extracardiac voltages, that can be measured non-invasively on the body surface.

We have discussed the principles that underlie currently practical electrocardiography, outlined its weaknesses, and described approaches to improving its capabilities. The most obvious limitation of the standard ECG, sparse spatial sampling, has motivated researchers to develop the cardiac mapping techniques described here, which are now widely utilized in experimental studies, and to a lesser extent in clinical applications. We have described a variety of the published analysis approaches and focused on the inverse solution, a means of generating estimated images of the electrical activity of the heart from image sequences of potentials recorded by body surface mapping. There are numerous aspects of cardiac electrical imaging of interest to signal processors; some of these are shared with other medical imaging modalities and others are not. We have emphasized both the analogies, as well as the important differences, with standard imaging processing.

Perhaps the main hurdle to more general use of clinical body surface mapping has been the paucity of techniques for unambiguous analysis of the resulting data. There are a number of research questions in this methodology that could benefit from further contributions from the signal processing community. Among these, we wish to emphasize the possibilities for better techniques for representation of these images, perhaps involving the adaptation of standard or emerging image processing techniques to the requisite non-regular and curved geometries, and involving more statistically-based, but local, characterizations. In turn, these representations could lead to improved feature extraction and the development of better quantitative measures for comparing electrical image sequences. In addition, in the case of high-density recordings from the cardiac surface, where wavefront propagation is a reasonable data model, there are many possibilities for careful application of array processing techniques; however we caution that the important differences between standard wave propagation models and cardiac propagation must be taken into account.

Finally, inverse solutions are a particularly promising area for interaction between signal processing and cardiac electrical imaging. Several key issues in inverse electrocardiography remain unresolved. For instance, the requirements of the inverse solution include a quantitative description of the torso geometry and conductivity, but the relationship between the accuracy of this description and that of the resulting inverse solution is not yet known, and numerical and even statistical characterizations of this relationship would be of great interest. Perhaps the most critical requirement for an inverse solution, a numerical means of constraining the ill-posed nature of the problem, is another important area of ongoing research. While the eventual capabilities and limitations of this modality are impossible to predict, it is clear that inverse solutions accurate enough for general clinical application will need to incorporate sophisticated techniques to impose physiologically realistic constraints as precisely as possible. Such solutions hold the promise of greatly improved characterization, quantification, and localization of cardiac abnormalities from non-invasive body surface measurements.

Acknowledgment: The authors wish to thank Robert Lux and Bruno Taccardi of the CVRTI and Milan Horacek of Dalhousie University for access to some of the data presented, and Quan Ni and Rick Gaudette for help in preparation of some of the figures.

References

[1] H.P. Selker. Coronary care unit triage decision aids: How do we know when they work? *Am. J. Med.*, 87:491–493, 1989.

[2] P. Kinias and H.A. Fozzard. Rapid ECG analysis and arrhythmis detection. In L.D. Cady, editor, *Computer Techniques in Cardiology*, pages 97–122. Marcel Dekker Inc., New York/Basel, 1979.

[3] H.K. Wolf, P.J. MacInnis, S. Stock, R.K. Helppi, and P.M. Rautaharju. Computer analysis of rest and exercise electrocardiograms. *Comp. & Biom. Res.*, pages 329–346, 1972.

[4] W.D. Anderson, N.B. Wagner, K.L. Lee, R.D. White, J. Yuschak, V.S. Behar, R.H. Selvester, R.E. Ideker, and G.S. Wagner. Evaluation of a QRS scoring system for estimating myocardial infarct size. VI: Identification of screening criteria for non-acute myocardial infarcts. *Am. J. Cardiol.*, 61:729–733, 1988.

[5] B. Taccardi. Distribution of heart potentials on the thoracic surface of normal human subjects. *Circ. Res.*, 1:341–351, 1963.

[6] B.R. Farr, B. Vondenbusch, J. Silny, G. Rau, and S. Effert. Localization of significant coronary arterial narrowings using body surface potential mapping during exercise stress testing. *Am. J. Cardiol.*, 5:528–530, 1987.

[7] L.S. Green, R.L. Lux, and C.W. Haws. Detection and localization of coronary artery disease with body surface mapping in patients with normal electrocardiograms. *Circ.*, 76:1290–1297, 1987.

[8] D.D. McPherson, B.M. Horáček, D.E. Johnstone, L.D. Lalonde, C.A. Spencer, and T.J. Montague. Q-wave infarction: Pathophysiology of body surface potential map and ventriculographic patterns in anterior and inferior groups. *Can. J. Cardiol.*, Supp. A:91A–98A, 1986.

[9] F. Kornreich, T.J. Montague, and P.M. Rautaharju. Location and magnitude of ST changes in acute myocardial infarction by analysis of body surface potential maps. *J. Electrocardiol.*, 25(supp):15, 1992.

[10] L. DeAmbroggi, B. Taccardi, and E. Macchi. Body surface maps of heart potential: Tentative localization of preexcited area of forty-two Wolff-Parkinson-White patients. *Circ.*, 54:251, 1976.

[11] J. Liebman, C.W. Thomas, and Y. Rudy. Conduction abnormalities and ventricular hypertrophy. In D.M. Mirvis, editor, *Body Surface Electrocardiographic Mapping*, pages 153–166. Kluwer Academic Publishers, Boston, Dordrecht, London, 1988.

[12] F. Kornreich, T.J Montague, P.M. Rautaharju, M. Kavadias, and B.M. Horáček. Identification of best electrocardiographic leads for diagnosing left ventricular hypertrophy by statistical analysis of body surface potential maps. *Am. J. Cardiol.*, 62:1285–1291, 1988.

[13] R.E. Ideker and R.C. Barr, editors. *Proceedings of the IEEE, special issue on electrical therapy of cardiac arrhythmias*, volume 84. IEEE, 1996.

[14] W. Müller, H. Windisch, and H. A. Tritthart. Fluorescent styryl dyes applied as fast optical probes of cardiac action potential. *Eur. Biophys. J*, 1:103–111, 1986.

[15] W. Merx, M.S. Yoon, and J Han. The role of local disparity in conduction and recovery time on ventricular vulnerability to fibrillation. *Am. Heart J.*, 94(5):603–610, 1977.

[16] L.S. Gettes. Effects of ischemia on cardiac electrophysiolgy. In Fozzard, H.E. *et al.*, editor, *The Heart and Cardiovascular System*, pages 1317–1341. Raven Press, New York, 1986.

[17] D.P. Zipes and J. Jalife, editors. *Cardiac Electrophysiology, From Cell to Bedside*. Grune & Stratton, New York, N.Y., 1989.

[18] C.S. Henriquez and A.A. Papazoglou. Using computer models to understand the roles of tissue structure and membrane dynamics in arrythmogenesis. *Proc. IEEE*, 84(3):334, 1996.

[19] D.D. Streeter and C. Ramon. Muscle pathway geometry in the heart wall. *J. Biomech. Eng*, 10:367–373, 1983.

[20] D. E. Roberts, L. T. Hersh, and A. M. Scher. Influence of cardiac fiber orientation on wavefront voltage, conduction velocity, and tissue resistivity in the dog. *Circ. Res.*, 44:701–712, 1979.

[21] B. Taccardi, E. Macchi, R.L. Lux, P.R. Ershler, S. Spaggiari, S. Baruffi, and Y. Vyhmeister. Effect of myocardial fiber direction on epicardial potentials. *Circ.*, 90:3076–3090, 1994.

[22] A.L. Goldberger and E. Goldberger. *Clinical Electrocardiography*. C.V. Mosby, 1986.

[23] J.M.T. De Bakker, M.J. Janse, F.J.L. Van Capelle, and D. Durrer. Endocardial mapping by simultaneous recording of endocardial electrograms during cardiac surgery for ventricular aneurysm. *J. Am. Coll. Cardiol.*, 2:947–953, November 1983.

[24] J.L. Cox, T.M. Daniel, and J.P. Boineau. The electrophysological time-course of acute myocardial ischemia and the effects of early coronary artery reperfusion. *Circ.*, 48:971–983, Nov 1973.

[25] G. Arisi, E. Macchi, S. Baruffi, S. Spaggiari, and B. Taccardi. Potential fields on the ventricaular surface of the exposed dog heart during normal excitation. *Circ. Res.*, 5:706–715, 1983.

[26] R.L. Lux. Mapping techniques. In P.W. Macfarlane and T.D. Veitch Lawrie, editors, *Comprehensive Electrocardiology*, volume 2, chapter 26, pages 1001–1014. Pergamon Press, 1989.

[27] Y. Watanabe. The state of body surface mapping in Japan. *J. Electrocardiol.*, 29-Supp.:110–120, 1995.

[28] C.F. Pieper and A. Pacifico. The epicardial field potential in dog: Implications for recording site density during epicardial mapping. *Pace*, 16:1263–1274, June 1993.

[29] R.C. Barr and M.S. Spach. Sampling rates required for digital recording of intracellular and extracellular cardiac potentials. *Circ.*, 5:40–48, 1977.

[30] B. Taccardi, R.L. Lux, R.S. MacLeod, P.R. Ershler, T.J. Dustman, and Y. Vhymeister. ECG waveforms and cardiac electric sources. *J. Electrocardiol.*, 29 Supp.:(in press), 1996.

[31] R.S. MacLeod, C.R. Johnson, and M.A. Matheson. Visualization tools for computational electrocardiography. In *Visualization in Biomedical Computing*, pages 433–444, Bellingham, Wash., 1992. Proc. SPIE 1808.

[32] R.S. MacLeod, C.R. Johnson, and M.A. Matheson. Visualizing bioelectric fields. *IEEE Comp. Graph. & Applic.*, 13(4):10–12, 1993.

[33] R.C. Barr and M.S. Spach. A comparison of measured epicardial potentials with epicardial potentials computed from body surface measurements in the intact dog. *Adv. Cardiol.*, 21:19–22, 1978.

[34] Y. Nagata. The influence of the inhomogeneities of electrical conductance within the torso on the electrocardiogram as evaluated from the view point of the transfer impedance vector. *Jap. Heart J.*, 11(5):489–505, 1970.

[35] L. DeAmbroggi and B. Taccardi. Current and potential fields generated by two dipoles. *Circ. Res.*, 27:910–911, 1970.

[36] D.M. Mirvis. Electrocardiographic QRS changes induced by acute coronary ligation in the isolated rabbit heart. *J. Electrocardiol.*, 12(2):141–150, 1979.

[37] B. Soucy, R.M. Gulrajani, and R. Cardinal. Inverse epicardial potential solutions with an isolated heart preparation. In *IEEE Engineering in Medicine and Biology Society 11th Annual International Conference*, pages 193–194. IEEE Press, 1989.

[38] P. Colli Franzone, L. Guerri, B. Taccardi, and C. Viganotti. The direct and inverse problems in electrocardiology. Numerical aspects of some regularization methods and applications to data collected in isolated dog heart experiments. *Lab. Anal. Numerica C.N.R.*, Pub. N:222, 1979.

[39] B.J. Messinger-Raport and Y. Rudy. Noninvasive recovery of epicardial potentials in a realistic heart-torso geometry. *Circ. Res.*, 66, 4:1023–1039, 1990.

[40] R.S. MacLeod, B. Taccardi, and R.L. Lux. The influence of torso inhomogeneities on epicardial potentials. In *IEEE Computers in Cardiology*, pages 793–796. IEEE Computer Society, 1994.

[41] R.S. MacLeod, B. Taccardi, and R.L. Lux. Electrocardiographic mapping in a realistic torso tank preparation. In *IEEE Engineering in Medicine and Biology Society 17th Annual International Conference*, pages 245–246. IEEE Press, 1995.

[42] S.M. Blanchard, R.J. Damiano, W.M. Smith, R.E. Ideker, and J.E. Lowe. Interpolating unipolar epicardial potentials from electrodes separated by increasing distances. *Pace*, 12:1938–1955, 1989.

[43] B.J.A. Schijvenaars, J.A. Kors, G. van Herpen, F. Kornreich, and J.H. van Bemmel. Interpolation of body surface potential maps. *J. Electrocardiol.*, 28 Suppl.:104–109, 1995.

[44] R. Moorhead II and Z Zhu. Signal processing aspects of scientific visualization. *IEEE signal processing magazine*, 1995.

[45] H. R. Grogin, M. L. Stanley, S. Eisenberg, B. M. Horacek, and M. D. Lesh. Body surface mapping for localization of accessory pathways in WPW syndrome. In *IEEE Computers in Cardiology*, page 255. IEEE Computer Society, 1992.

[46] C.L. Nikias, M.R. Raghuveer, J.H. Siegel, and M. Fabian. The zero-delay wavenumber spectrum estimation for the analysis of array ECG signals — an alternative to isopotential mapping. *IEEE Trans Biomed. Eng.*, BME-33:435–452, 1986.

[47] D.H. Brooks, H. Krim, J.C. Pesquet, and R.S. MacLeod. Best basis segmentation of ECG signals using novel optimality criteria. In *Proc. ICASSP-96*, 1996.

[48] F.N. Wilson, A.G. MacLeod, P.S. Barker, and F.D. Johnston. The determination and the significance of the areas of the ventricular deflections of the electrocardiogram. *Am. Heart J.*, 10:46, 1934.

[49] R. Plonsey. A contemporary view of the ventricular gradient of Wilson. *J. Electrocardiol.*, 12:337–341, 1979.

[50] D.B. Geselowitz. The ventricular gradient revisited: Relation to the area under the action potential. *IEEE Trans Biomed. Eng.*, BME-30:76–77, 1983.

[51] E.J. Berbari, D. Ramachandran, P. Lander, and D. Geselowitz. Identifying uncertainty in epicardial activation maps. In *IEEE Computers in Cardiology*, pages 423–426. IEEE Computer Society, 1992.

[52] C.W. Haws and R.L. Lux. Correlation between *in vivo* transmembrane action potentials and activation-recovery intervals from electrograms: Effects of interventions that alter repolarization time. *Circ.*, 81:281–288, 1990.

[53] A.R. Grüntzig, R.K. Myler, and E.S. Hanna. Coronary transluminal angioplasty. *Circ.*, 56:III–84, 1977.

[54] R.L. Lux. Karhunen-Loeve representation of ECG data. *J. Electrocardiol.*, 25(supp):195, 1992.

[55] R.L. Lux, K. Evans, M.J. Burgess, R.F. Wyatt, and J.A. Abildskov. Redundancy reduction for improved display and analysis of body surface potential maps: I. Spatial compression. *Circ. Res.*, 49:186–196, 1981.

[56] K. Evans, R.L. Lux, M.J. Burgess, R.F. Wyatt, and J.A. Abildskov. Redundancy reduction for improved display and analysis of body surface potential maps: II. Temporal compression. *Circ. Res.*, 49:197–203, 1981.

[57] C.L. Hubley-Kozey, B. Mitchell, M.J. Gardner, J.W. Warren, C.J. Penney, E.R. Smith, and B.M. Horáček. Spatial features in body surface potentials maps can identify patients with a history of sustained ventricular tachycardia. *Circ.*, 92:1825–1838, 1995.

[58] F. Kornreich, T.J. Montague, and P.M. Rautaharju. Body surface potential mapping of ST segment changes in acute myocardial infarction: Implications for ECG enrollment criteria for thrombolytic therapy. *Circ.*, 87(3):773, 1993.

[59] R.L. Lux and R.S. Macleod. Estimating electrocardiographic distributions from small numbers of leads. *J. Electrocardiol.*, 28 Suppl.:92–98, 1995.

[60] P.V. Bayly, E.E. Johnson, P.D. Wolf, H.S. Greenside, W.S. Smith, and R.E. Ideker. A quantitative measurement of spatial order in ventricular fibrillation. *J. Cardiovasc. Electrophysiol.*, 4:533–546, 1993.

[61] P. Lander and E. Berbari. Contouring of epicardial activation using spatial autocorrelation estimates. In *IEEE Comp. in Card.*, pages 541–544. IEEE Computer Society, 1992.

[62] P.V. Bayly, R.E. Hillsley, P.D. Gerstle, P.D. Wolf, W.M Smith, and R.E. Ideker. Estimation of propagation speed during ventricular fibrillation from frequency-wavenumber power spectra. In *IEEE Computers in Cardiology*, pages 161–164. IEEE Computer Society, 1994.

[63] J.H. Siegel, C.L. Nikias, M.R. Raghuveer, M. Fabian, K.C. Goh, and D. Sanford. Epicardial electrical activity analyzed via frequency wavenumber spectrum estimation for the characterization of arrhythmiagenic states. *J. Electrocardiol.*, 20(5):329–351, 1987.

[64] S. Abboud, R.J. Cohen, A. Selwyn, P. Ganz, D. Sadeh, and P.L. Friedman. Detection of transient myocardial ischemia by computer analysis of standard and signal-averaged high-frequency electrocardiograms in patients undergoing percutaneous transluminal coronary angioplasty. *Circ.*, 76:585–596, 1987.

[65] D.M. Davenport, D.H. Brooks, and R.S. MacLeod. Experimentally derived realistic constraints on epicardial potential distributions. In *Proc. 21st N.E. Bioengineering Conference*, Bar Harbour, ME, March 1995.

[66] D.H. Brooks, C.L Nikias, and J.H. Siegel. An inverse solution in electrocardiography in the frequency domain. In *IEEE Engineering in Medicine and Biology Society 10th Annual International Conference*, pages 970–971, 1988.

[67] R.S. MacLeod, D.H. Brooks, H. On, H. Krim, R.L. Lux, and F. Kornreich. Analysis of PTCA-induced ischemia using both an electrocardiographic inverse solution and the wavelet transform. *J. Electrocardiol.*, 27 Suppl.:90–96, 1994.

[68] D.H. Brooks, R.S. MacLeod, and H. Krim. Analysis of changes in body surface potentials during PTCA-induced ischemia using the temporal wavelet transform. In *IEEE Computers in Cardiology*, pages 329–332. IEEE Computer Society, 1994.

[69] D.H. Brooks, H. On, and R.S. MacLeod. Spatio-temporal wavelet analysis of body surface potential maps during PTCA-induced ischemia. In *IEEE Engineering in Medicine and Biology Society 16th Annual International Conference*, pages 1208–1209, 1994.

[70] R. Murray, S. Kadambe, and G.F. Boudreaux-Bartels. Extensive analysis of a QRS detector based on the dyadic wavelet transform. In *Proc. IEEE Symposium on Time-Frequency and Time-Scale*, pages 540–543. IEEE Press, 1994.

[71] G. Li, C. Zheng, and C. Tai. Detection of ECG characteristic points using wavelet transforms. *IEEE Trans Biomed. Eng.*, 42:21–28, 1995.

[72] D.H. Brooks, R.S. MacLeod, R.V. Chary, R.J. Gaudette, and H. Krim. Temporal and spatial analysis of potential maps via multi-resolution decompositions. *j-JE*, in press 1996.

[73] D.S. Khoury, B. Taccardi, R.L. Lux, P.R. Ershler, and Y. Rudy. Reconstruction of endocardial potentials and activation sequences from intracavity probe measurements. *Circ.*, 91:845–863, 1995.

[74] R.M. Gulrajani, P. Savard, and F.A. Roberge. The inverse problem in electrocardiography: Solutions in terms of equivalent sources. *CRC Crit. Rev. Biomed. Eng.*, 16:171–214, 1988.

[75] Y. Rudy and B. J Messinger-Rapport. The inverse problem in electrocardiography: solutions in terms of epicardial potentials. *CRC Crit. Rev. in Biomed. Eng.*, 16:215–268, 1988.

[76] Y. Yamashita. Theoretical studies on the inverse problem in electrocardiography and the uniqueness of the solution. *IEEE Trans Biomed Eng*, BME-29:719–725, 1982.

[77] C.R. Johnson, R.S. MacLeod, and P.R. Ershler. A computer model for the study of electrical current flow in the human thorax. *Comp. in Biol. & Med.*, 22:305–323, 1992.

[78] J.A. Schmidt, C.R. Johnson, J.A. Eason, and R.S. MacLeod. Applications of automatic mesh generation and adaptive methods in computational medicine. In J. Flaherty and I. Babuska, editors, *Modeling, Mesh Generation, and Adaptive Methods for Partial Differential Equations*, pages 367–394. Springer Verlag, 1994.

[79] Y. Rudy and R. Plonsey. The effects of variations in conductivity and geometrical parameters on the electrocardiogram, using an eccentric spheres model. *Circ. Res.*, 44(1):104–111, 1979.

[80] Y. Rudy and B.J. Messinger-Rapport. The inverse solution in electrocardiography: Solutions in terms of epicardial potentials. *CRC Crit. Rev. Biomed. Eng.*, 16:215–268, 1988.

[81] P.C. Stanley, T.C. Pilkington, and M.N. Morrow. The effects of thoracic inhomogeneities on the relationship between epicardial and torso potentials. *IEEE Trans Biomed. Eng.*, BME-33:273–284, 1986.

[82] A. Pullan. A high-order coupled finite/boundary element torso model. *IEEE Trans Biomed. Eng.*, 43(3):292–298, 1996.

[83] G.J. Huiskamp and A. Van Oosterom. Tailored versus geometry in the inverse problem of electrocardiography. *IEEE Trans Biomed. Eng.*, 36:827–835, 1989.

[84] R.N. Klepfer, C.R. Johnson, and R.S. MacLeod. The effects of inhomogeneities and anisotropies on electrocardiographic fields: A three-dimensional finite elemental study. In *IEEE Engineering in Medicine and Biology Society 17th Annual International Conference*, pages 233–234. IEEE Press, 1995.

[85] H.S. Oster and Y. Rudy. The use of temporal information in the regularization of the inverse problem of electrocardiography. *IEEE Trans Biomed. Eng.*, 39(1):65–75, 1992.

[86] D.H. Brooks, G.M. Maratos, G. Ahmad, and R.S. MacLeod. The augmented inverse problem of electrocardiography: combined time and space regularization. In *IEEE Engineering in Medicine and Biology Society 15th Annual International Conference*, pages 773–774. IEEE Press, 1993.

[87] D.H. Brooks, G. Ahmad, and R.S. MacLeod. Multiply constrained inverse electrocardiology: Combining temporal, multiple spatial, and and iterative regularization. In *IEEE Engineering in Medicine and Biology Society 16th Annual International Conference*, pages 137–138. IEEE Computer Society, 1994.

[88] G.F. Ahmad, D.H. Brooks, C.A. Jacobson, and R. S MacLeod. Constraint evaluation in inverse electrocardiography using convex optimization. In *IEEE Engineering in Medicine and Biology Society 17th Annual International Conference*, pages 209–210. IEEE Press, 1995.

[89] J.J.M. Cuppen and A. van Oosterom. Model studies with the inversely calculated isochrones of ventricular depolarization. *IEEE Trans Biomed. Eng.*, BME-31:652–659, 1984.

[90] F. Greensite, Y.J. Qian, E. Alzarka, and F. Jaffer. Deconvolution without regularization in inverse electrocardiography. In *IEEE Engineering in Medicine and Biology Society 15th Annual International Conference*, pages 769–770. IEEE Computer Society, 1993.

[91] F. Greensite. Demonstration of "discontinuities" in the true derivative of body surface potential, and their prospective role in noninvasive imaging of the ventricular surface activation map. *IEEE Trans Biomed. Eng.*, 40(12):1210–1218, 1993.

[92] D.H. Brooks, C.L Nikias, and J.H. Siegel. An inverse solution in electrocardiography in the frequency domain. In *IEEE EMBS 10th Ann. Int. Conf.*, pages 970–971, 1988.

[93] P.C. Hansen. Analysis of discrete ill-posed problems by means of the L-curve. *SIAM Review*, 34(4):561–580, 1992.

[94] C. W. Groetsch. *The Theory of Tikhonov Regularization for Fredholm Equations of the First Kind*. Pitman, Boston, 1984.

[95] P. Colli Franzone, L. Guerri, S. Tentonia, C. Viganotti, S. Spaggiari, and B. Taccardi. A numerical procedure for solving the inverse problem of electrocardiography. Analysis of the time-space accuracy from *in vitro* experimental data. *Math. Biosci.*, 77:353, 1985.

[96] R.C. Barr and M.S. Spach. Inverse calculation of QRS-T epicardial potentials from body surface potential distributions for normal and ectopic beats in the intact dog. *Circ. Res.*, 42:661–675, 1978.

[97] B.J. Messinger-Rapport and Y. Rudy. Regularization of the inverse problem in electrocardiography: A model study. *Math. Biosci.*, 89:79–118, 1988.

[98] I. Iakovidis and R.M. Gulrajani. Regularization of the inverse epicardial solution using linearly constrained optimization. In *IEEE Engineering in Medicine and Biology Society 13th Annual International Conference*, pages 698–699. IEEE Press, 1991.

[99] A.V. Shahidi, P. Savard, and R. Nadeau. Forward and inverse problems of electrocardiography: Modeling and recovery of epicardial potentials in humans. *IEEE Trans Biomed. Eng.*, BME-41(3):249–256, 1994.

[100] C.R. Johnson and R.S. MacLeod. Local regularization and adaptive methods for the inverse Laplace problem. In D.N. Ghista, editor, *2nd Gauss Symposium: Medical Mathematics and Physics*. Vieweg-Verlag, Wiesbaden, 1996. (in press).

[101] R.S. MacLeod, C.R. Johnson, M.J. Gardner, and B.M. Horáček. Localization of ischemia during coronary angioplasty using body surface potential mapping and an electrocardiographic inverse solution. In *IEEE Computers in Cardiology*, pages 251–254. IEEE Press, 1992.

[102] F Greensite, Y-J Qian, and G. Huiskamp. Myocardial activation imaging: a new theorem and its implications. In *Proc. 17th Ann. Int. Conf. IEEE EMBS*, 1995.

[103] G.F Ahmad, D.H. Brooks, and R.S. MacLeod. An admissible solution approach to inverse electrocardiography. *Ann. Biomed. Eng.*, submitted 1996.

[104] D.C. Youla. Mathematical theory of image restoration by the method of convex projections. In H. Stark, editor, *Image Recovery: Theory and Application*. Academic Press, 1987.

List of Figures

1 Examples of electric potentials from the heart. Top panel contains a schematic electrocardiogram (ECG), with standard labels for each wave; middle panel shows an electrogram recorded from the outer surface of a canine heart with the characteristic intrinsic deflection marked; and the bottom panel contains schematic diagrams of action potentials from the ventricular myocardium (heart muscle). The alignment of the signals is realistic in that the QRS complex in the ECG reflects the range of upstrokes of all action potentials in the ventricles while electrograms are more selectively sensitive to tissue close to the electrode. 32

2 Epicardial and torso tank surface potentials recorded from an isolated heart in an electrolytic torso tank. The upper panel shows the epicardial distribution and the lower the torso tank distribution from the same time instant and from the same view. The heart in the upper figure is aligned as it was while suspended in the tank, but scaled severalfold for display purposes. The red dot in each map indicates the location of the two time signals shown at right. The color-bars below the two time signals show the mapping from potentials to color. 33

3 Samples of measured potentials from the body surface (panel a) and outer surface of the heart (panel b) to illustrate the diversity of waveforms. The four body surface signals were recorded simultaneously from different locations on the torso of the same subject under identical recording conditions. The four heart surface recordings were also simultaneously recorded, here from a canine ventricle using a 3 cm square array of electrodes 34

4 Sequence of maps based on canine epicardial data. The electrode array contained 21×25 electrodes regularly spaced at 2.0 mm separation and sewn into a nylon sock. Scaling—and thus contour spacing—is local to each frame such that the colors span the range of measured potentials. The 4 leftmost maps are isopotential instant maps from the same heartbeat. In these maps the positive potentials are mapped to red and negative potentials are mapped to blue. The time signal below each map corresponds to the location in the maps marked by the red dot and indicates how the maps progress through the beat. The rightmost column of maps were derived from the entire beat and represent the activation times (upper map) and recovery times (lower map) with scaling as indicated in the legends. 35

5 Sequence of epicardial maps from the whole heart. Electrode array contains 490 electrodes on semi-regular, curved grid over the entire ventricles. Red outlines show the location of major coronary arteries. Color coding for potentials is local to each instant ranging from dark blue for most negative potentials, through green, yellow, to red representing the most postive values. The time signal below each map is marked by a vertical line to show progress through the beat. 36

6 Sequence of isopotential instant maps from the body surface. Electrode array contained 117 leads with weighted spacing (higher density of coverage on the anterior surface) and irregular spacing. The left-hand map of each pair shows the anterior view, the right-hand map shows the posterior view. Positive potentials are coded in red, negative in blue and the scaling is local to each map. The instant in time for each map in the sequence is indicated by the vertical line on the ECG below each map pair. The labeled red dot indicates the location of this ECG. 37

7 KL transform applied to epicardial distributions. The upper four maps depict the first four eigenmaps derived from all the frames of the single beat shown in Figure 4. The lower two rows show reconstructed isopotential instant maps from two of the time instants shown in Figure 4; the left-hand map of each of these pairs are reconstructed from only the first four eigenmaps while the map in right-hand panel used the first 12 eigenmaps. 38
8 The singular value spectra of two different forward solution matrices: panel (a) was computed based on a realistic model of human anatomy, while panel (b) was based on a torso-shaped electrolytic tank with a canine heart suspended inside as described in the text. Note that the singular values are plotted on a log scale. 39
9 Isointegral and inverse solution results from a patient during coronary angioplasty (PTCA), as described in the text. The top panel contains two isointegral maps from the QRST segment, and their difference. The left map (A) originates from signals measured before inflation of the PTCA balloon while the middle map (B) is the same integral from a beat recorded at the latter, peak phase of the inflation; the rightmost map is the difference (peak- minus pre-inflation). These maps have been projected onto a two-dimensional surface, with the anterior torso on the left of each map and the posterior on the right. In the lower part of the figure, all distributions shown are isopotential instant maps, also from the same pre-inflation (panel A) and peak-inflation (Panel B) beats. The torso maps were measured, but the epicardial maps in the lower right portion of each panel contain estimates based on inverse calculations. The red areas denote positive potential, the blue denote negative potential and the green/yellow colors span the region of small potential values near zero. The arrow indicates the approximate location of the angioplasty balloon. 40

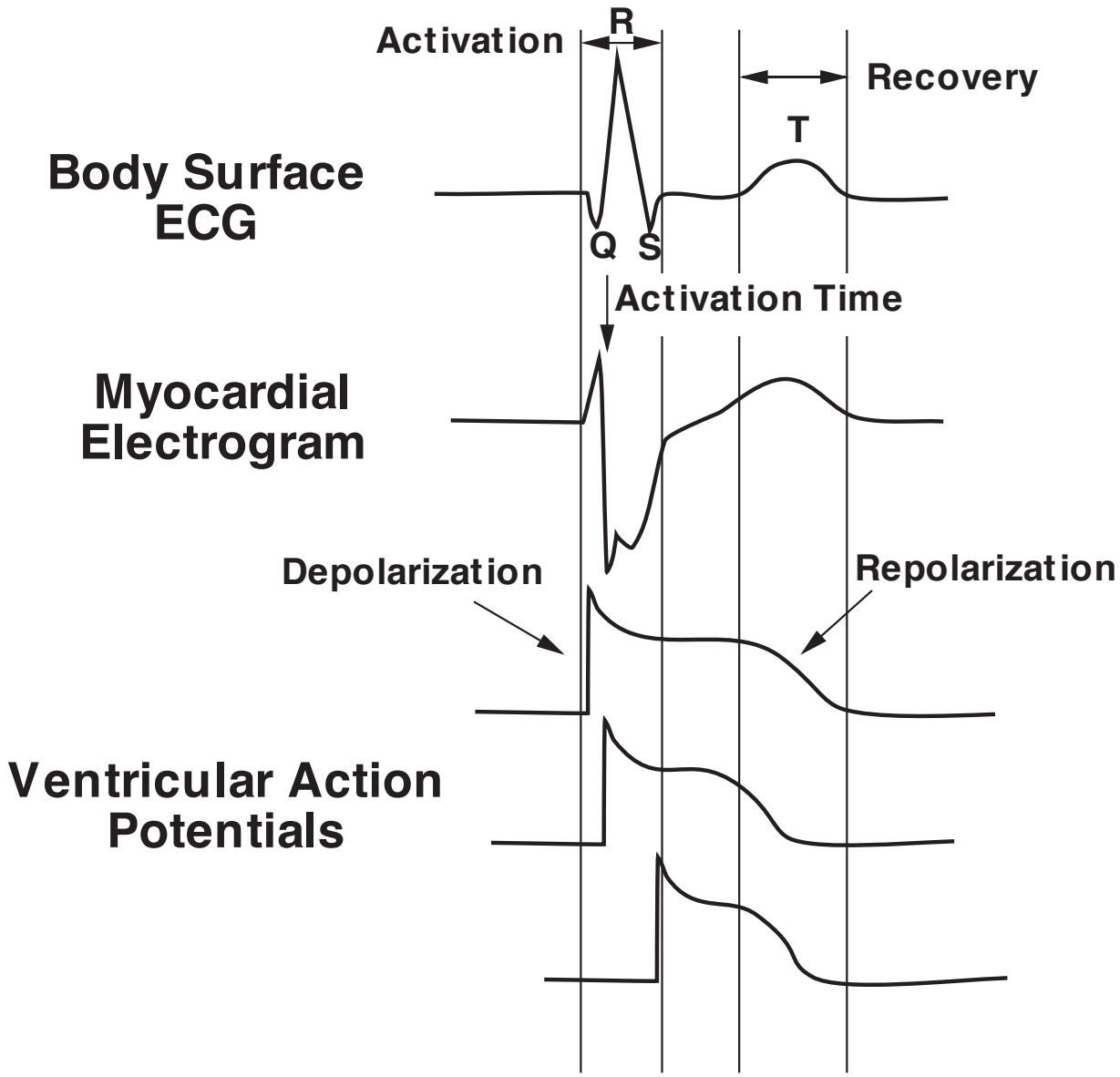

Figure 1: Examples of electric potentials from the heart. Top panel contains a schematic electrocardiogram (ECG), with standard labels for each wave; middle panel shows an electrogram recorded from the outer surface of a canine heart with the characteristic intrinsic deflection marked; and the bottom panel contains schematic diagrams of action potentials from the ventricular myocardium (heart muscle). The alignment of the signals is realistic in that the QRS complex in the ECG reflects the range of upstrokes of all action potentials in the ventricles while electrograms are more selectively sensitive to tissue close to the electrode.

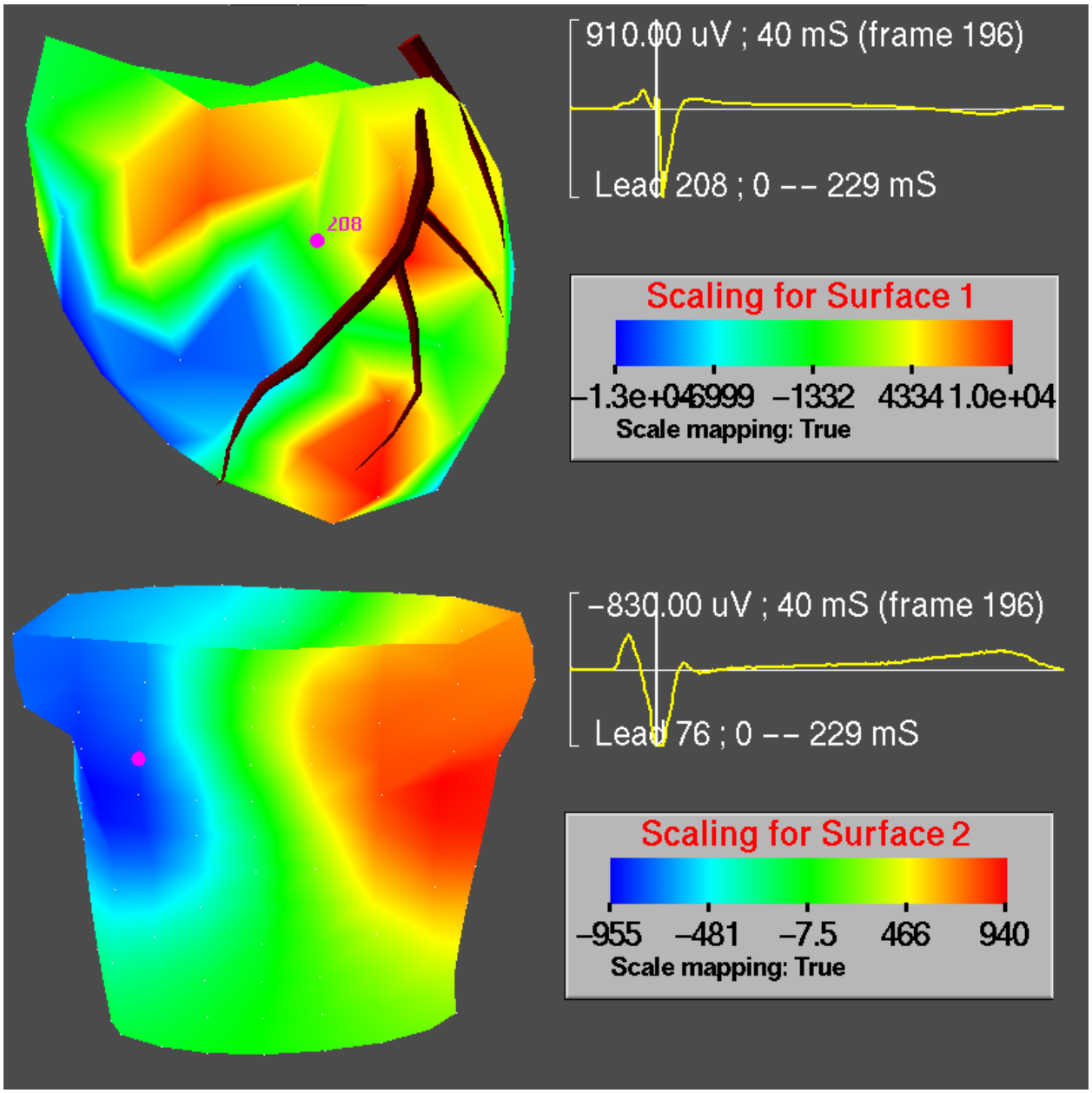

Figure 2: Epicardial and torso tank surface potentials recorded from an isolated heart in an electrolytic torso tank. The upper panel shows the epicardial distribution and the lower the torso tank distribution from the same time instant and from the same view. The heart in the upper figure is aligned as it was while suspended in the tank, but scaled severalfold for display purposes. The red dot in each map indicates the location of the two time signals shown at right. The color-bars below the two time signals show the mapping from potentials to color.

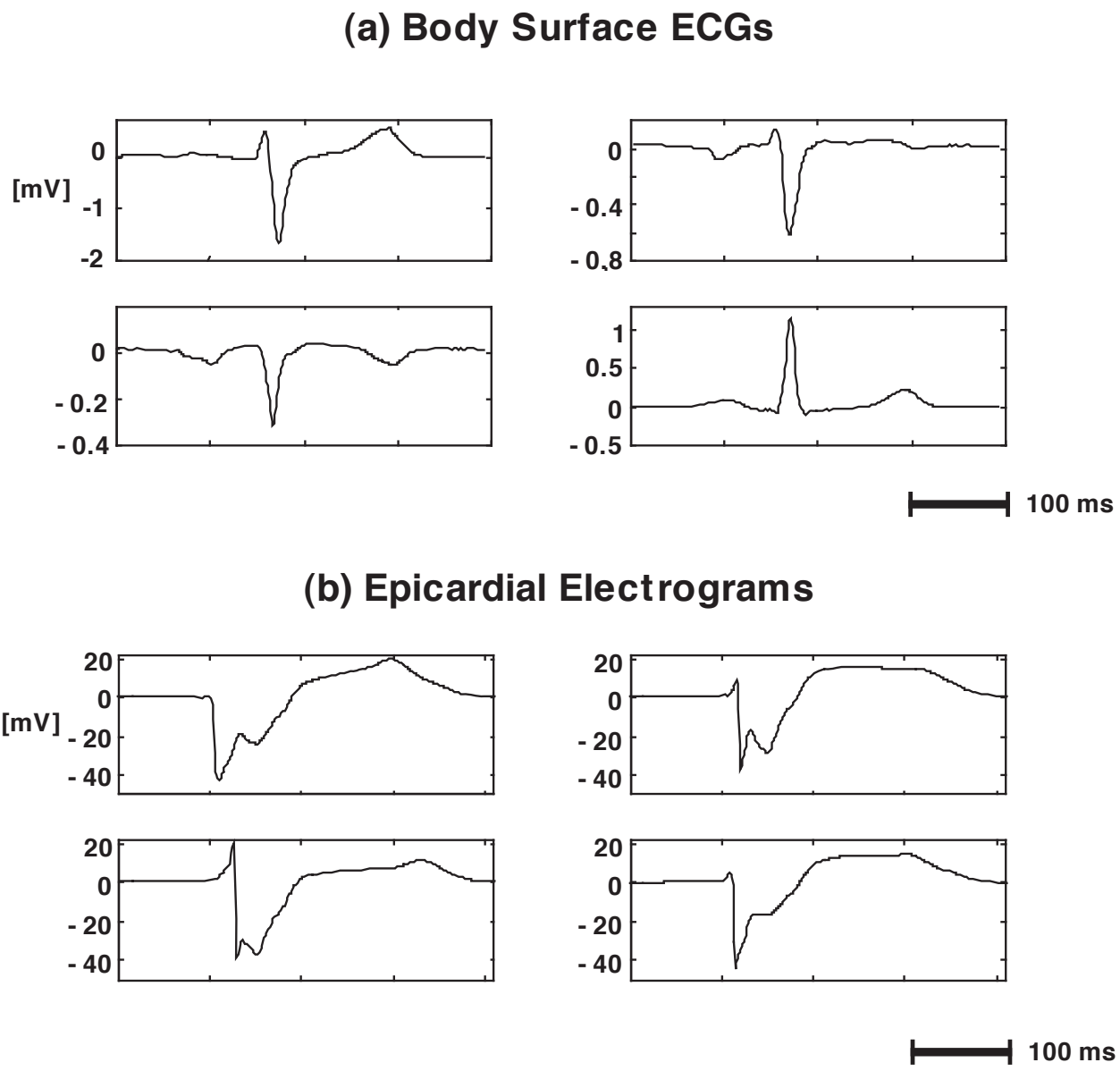

Figure 3: Samples of measured potentials from the body surface (panel a) and outer surface of the heart (panel b) to illustrate the diversity of waveforms. The four body surface signals were recorded simultaneously from different locations on the torso of the same subject under identical recording conditions. The four heart surface recordings were also simultaneously recorded, here from a canine ventricle using a 3 cm square array of electrodes

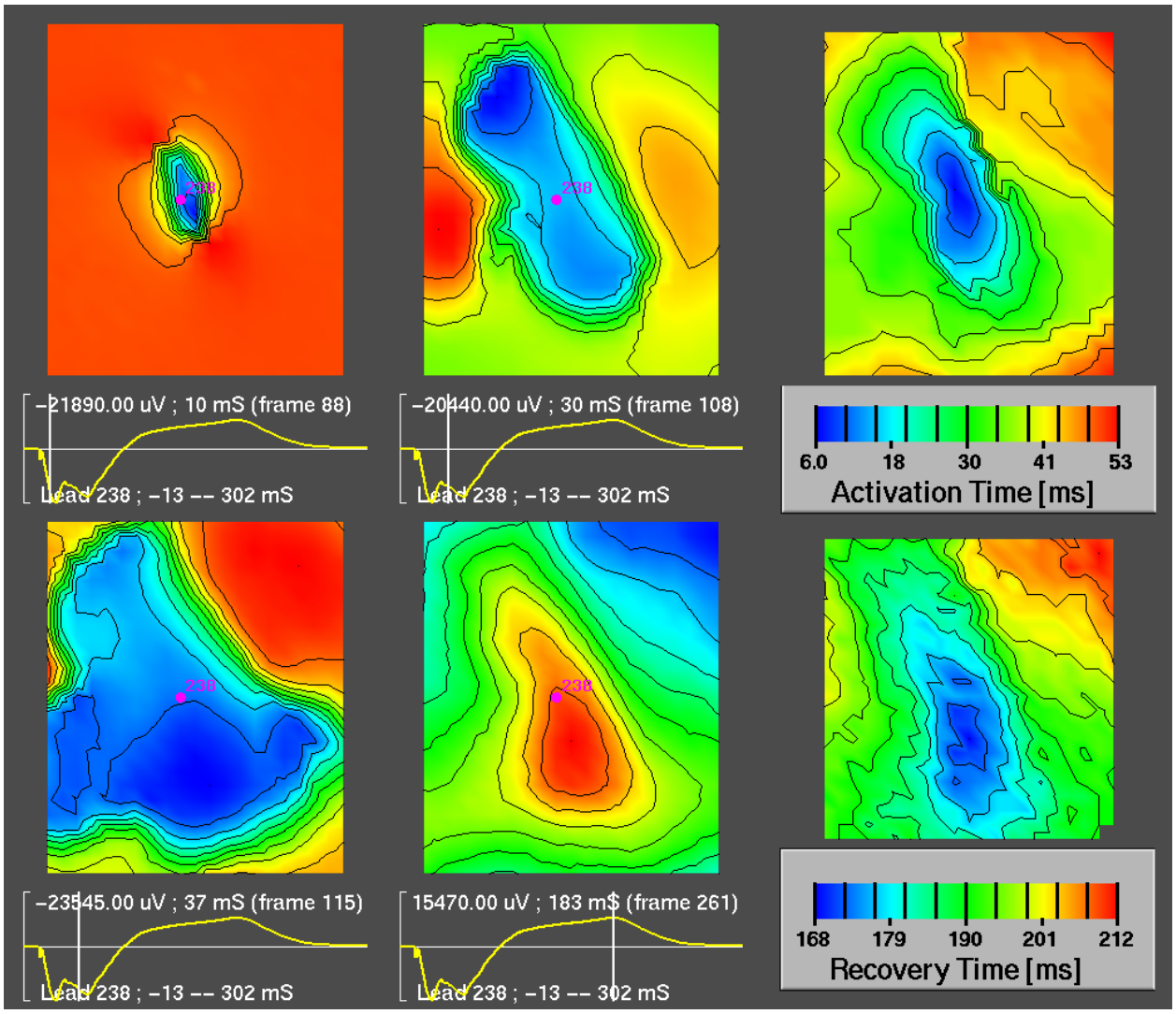

Figure 4: Sequence of maps based on canine epicardial data. The electrode array contained 21 × 25 electrodes regularly spaced at 2.0 mm separation and sewn into a nylon sock. Scaling—and thus contour spacing—is local to each frame such that the colors span the range of measured potentials. The 4 leftmost maps are isopotential instant maps from the same heartbeat. In these maps the positive potentials are mapped to red and negative potentials are mapped to blue. The time signal below each map corresponds to the location in the maps marked by the red dot and indicates how the maps progress through the beat. The rightmost column of maps were derived from the entire beat and represent the activation times (upper map) and recovery times (lower map) with scaling as indicated in the legends.

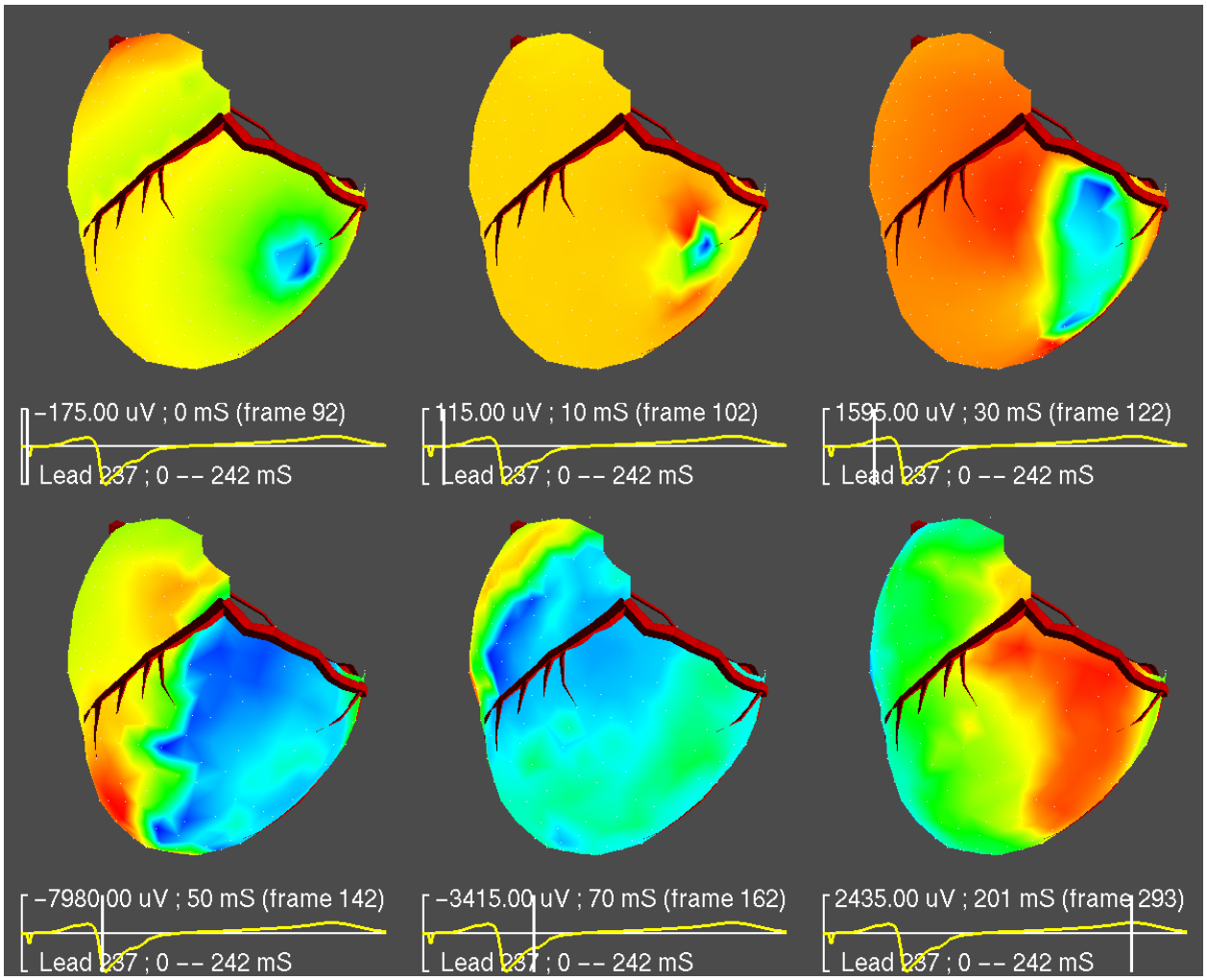

Figure 5: Sequence of epicardial maps from the whole heart. Electrode array contains 490 electrodes on semi-regular, curved grid over the entire ventricles. Red outlines show the location of major coronary arteries. Color coding for potentials is local to each instant ranging from dark blue for most negative potentials, through green, yellow, to red representing the most postive values. The time signal below each map is marked by a vertical line to show progress through the beat.

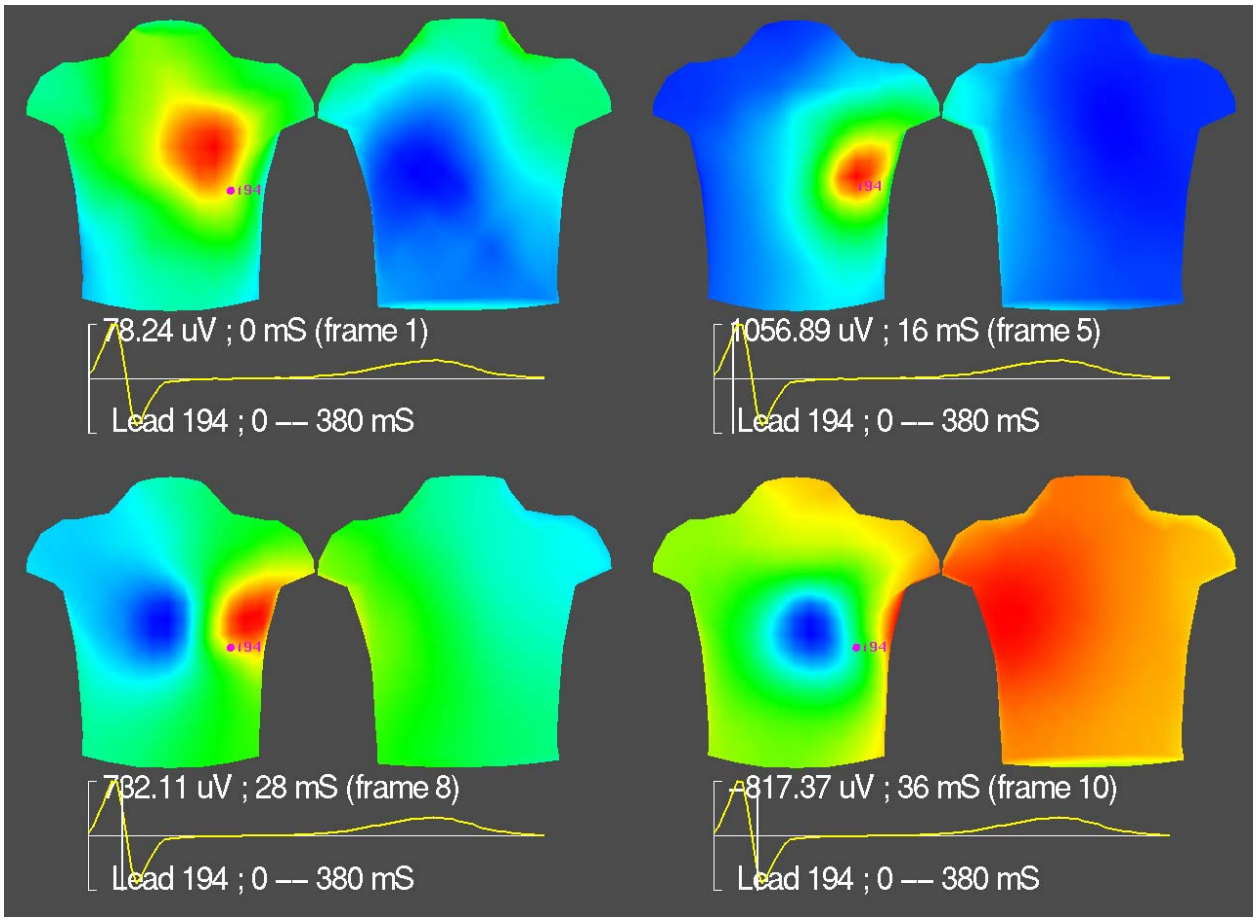

Figure 6: Sequence of isopotential instant maps from the body surface. Electrode array contained 117 leads with weighted spacing (higher density of coverage on the anterior surface) and irregular spacing. The left-hand map of each pair shows the anterior view, the right-hand map shows the posterior view. Positive potentials are coded in red, negative in blue and the scaling is local to each map. The instant in time for each map in the sequence is indicated by the vertical line on the ECG below each map pair. The labeled red dot indicates the location of this ECG.

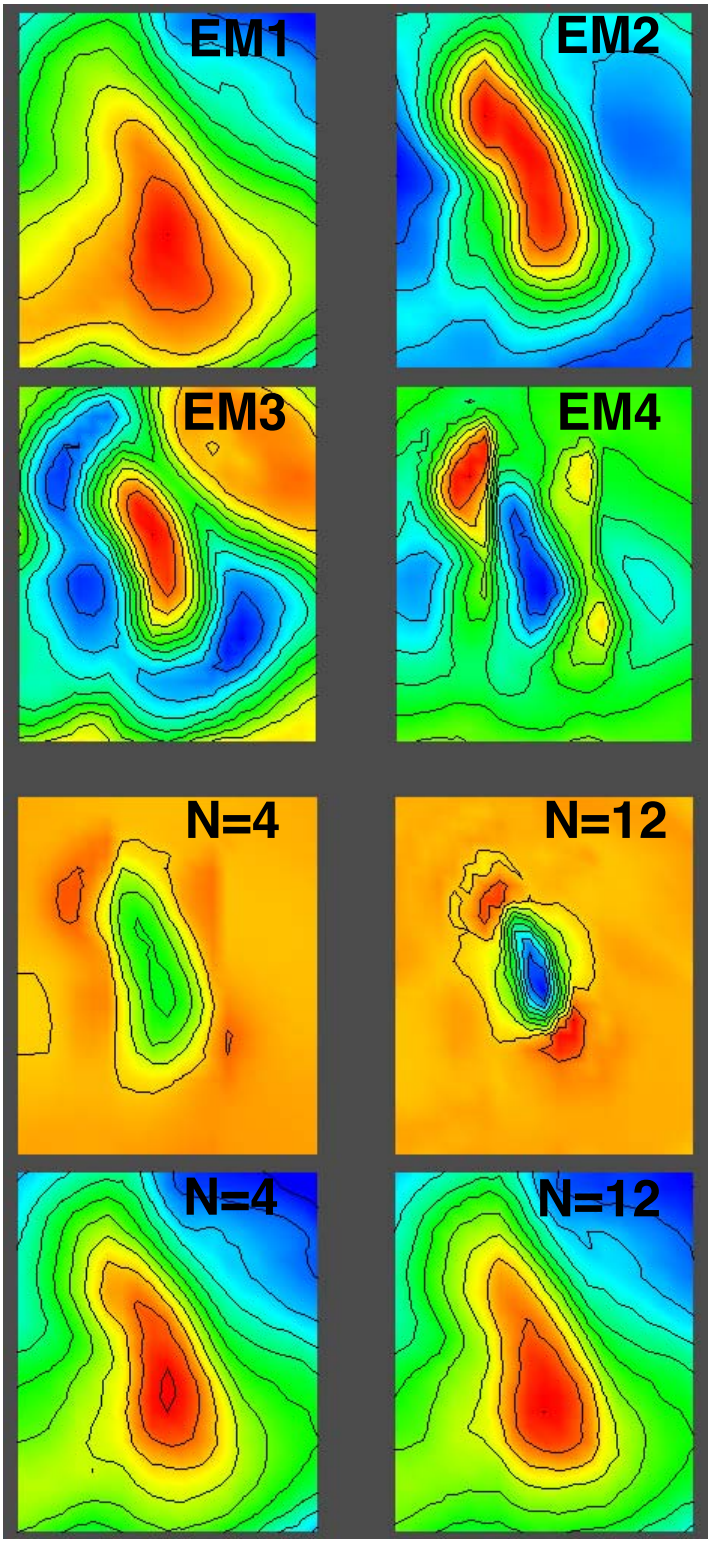

Figure 7: KL transform applied to epicardial distributions. The upper four maps depict the first four eigenmaps derived from all the frames of the single beat shown in Figure 4. The lower two rows show reconstructed isopotential instant maps from two of the time instants shown in Figure 4; the left-hand map of each of these pairs are reconstructed from only the first four eigenmaps while the map in right-hand panel used the first 12 eigenmaps.

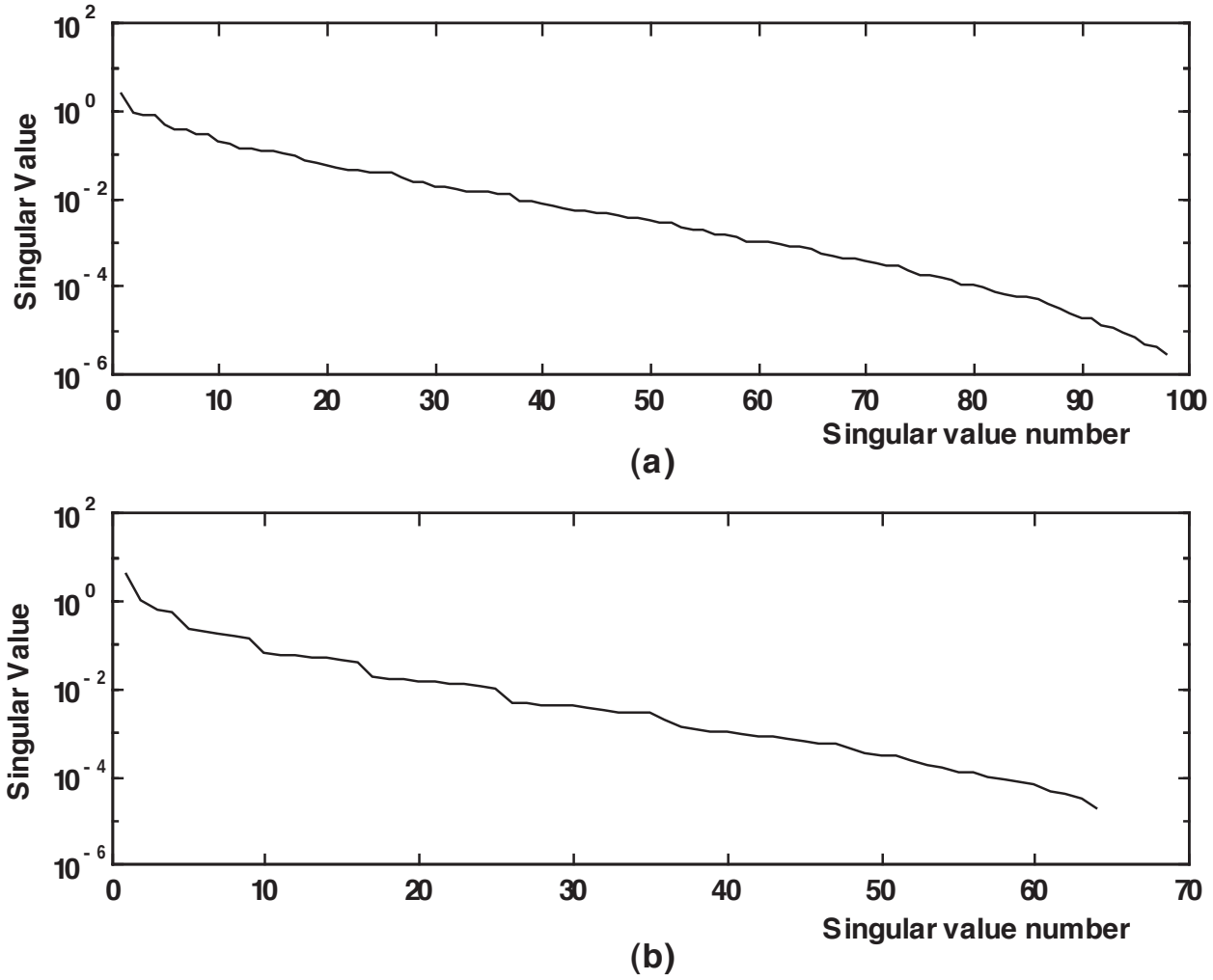

Figure 8: The singular value spectra of two different forward solution matrices: panel (a) was computed based on a realistic model of human anatomy, while panel (b) was based on a torso-shaped electrolytic tank with a canine heart suspended inside as described in the text. Note that the singular values are plotted on a log scale.

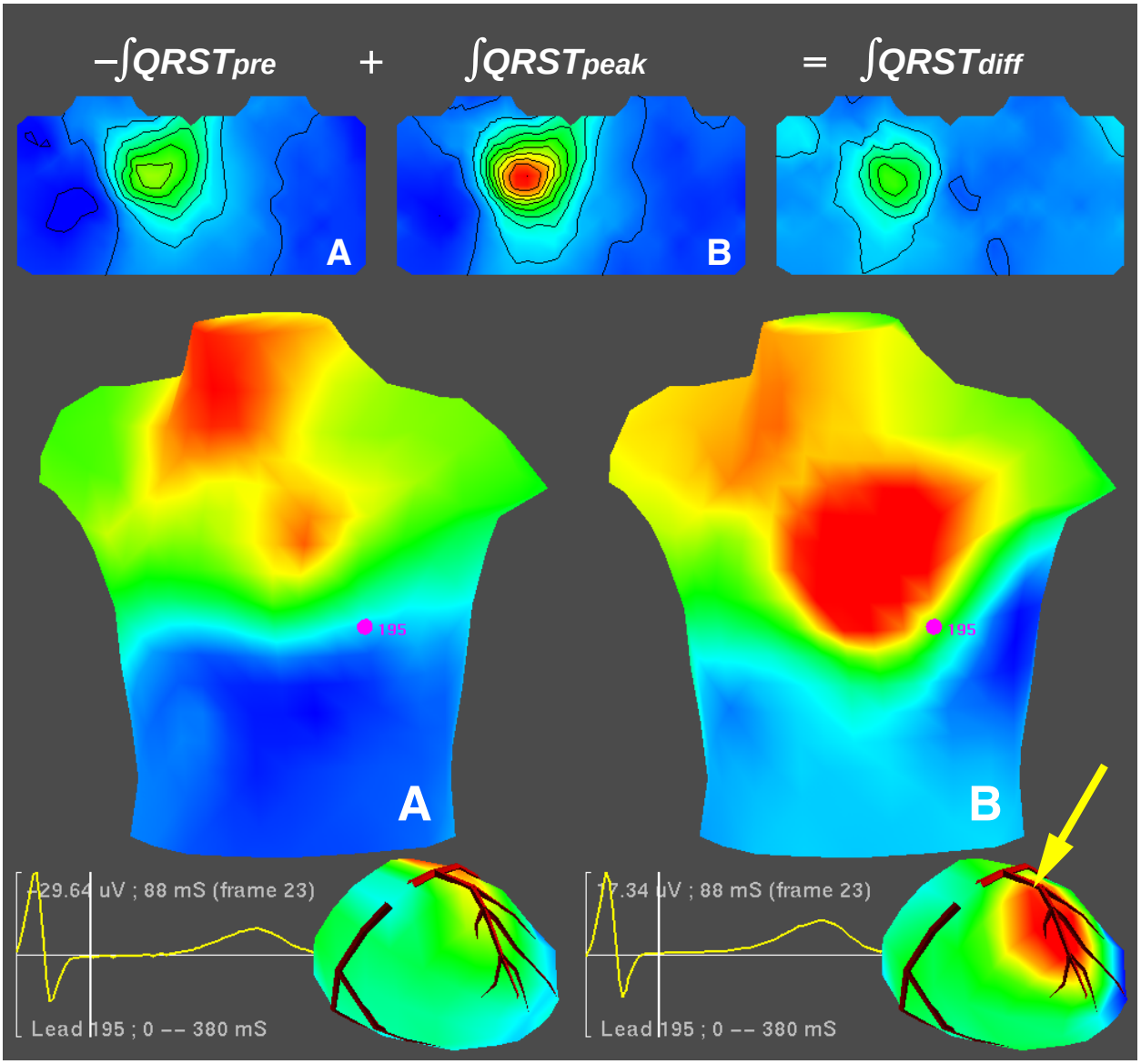

Figure 9: Isointegral and inverse solution results from a patient during coronary angioplasty (PTCA), as described in the text. The top panel contains two isointegral maps from the QRST segment, and their difference. The left map (A) originates from signals measured before inflation of the PTCA balloon while the middle map (B) is the same integral from a beat recorded at the latter, peak phase of the inflation; the rightmost map is the difference (peak- minus pre-inflation). These maps have been projected onto a two-dimensional surface, with the anterior torso on the left of each map and the posterior on the right. In the lower part of the figure, all distributions shown are isopotential instant maps, also from the same pre-inflation (panel A) and peak-inflation (Panel B) beats. The torso maps were measured, but the epicardial maps in the lower right portion of each panel contain estimates based on inverse calculations. The red areas denote positive potential, the blue denote negative potential and the green/yellow colors span the region of small potential values near zero. The arrow indicates the approximate location of the angioplasty balloon.